EUROPEAN ORGANIZATION FOR NUCLEAR RESEARCH

CERN-EP/89-140
November 2nd, 1989

The τ-charm Factory

Jasper Kirkby

CERN, Geneva, Switzerland

Abstract

We describe the status of a new experiment that will carry out precise studies of the third generation leptons, $\tau^{\pm}$ and ν_{τ}; the second generation quark family, through the decays of $D^{\pm}$, D^0 and $D_s^{\pm}$; and the spectrum of gluonic and other new light particles in the decays of J/ψ and ψ'. The experiment – the τ-charm Factory (τcF) – involves a high-resolution detector integrated with an intense e^+e^- collider operating in the energy range $3.0 \leq E_{cm} \leq 4.25$ GeV with a maximum luminosity $10^{33}\,\mathrm{cm}^{-2}\mathrm{s}^{-1}$.

Lectures given at the
XVII International Meeting on Fundamental Physics
Lekeitio, Vizcaya, Spain, 23-29 April 1989

Since this talk was given, a τ-charm Workshop took place at SLAC, 23-27 May 1989. With the expertise of 200 physicists, drawn from a dozen countries, an evaluation of the τ-charm physics prospects was made, along with a detailed investigation of the feasibility of the machine and the detector. The outcome was broad recognition both of the importance of a renewed, high precision, study of τ-charm physics and also of the suitability of an e^+e^- collider operating near τ-charm threshold for such studies. Furthermore, all the ingredients for the τ-charm Factory machine were considered to be realistic and, given careful design and engineering, they can be assembled into a working machine with a luminosity $\gtrsim 10^{33}\,\mathrm{cm}^{-2}\mathrm{s}^{-1}$. Finally, it was agreed that a detector that meets the physics requirements can be built with present technologies and that its performance will represent a substantial improvement relative to previous detectors at this energy. The results of these studies are contained in the *Proceedings of the Tau Charm Workshop*[1]. Inevitably the material presented in this paper has been updated by the findings of this Workshop, and the interested reader is directed to ref.[1] for further details and a comprehensive list of references.

In the first section of this paper, we emphasize the important future rôle of dedicated e^+e^- collider factories. This is followed by the considerations that lead to the proposed machine as the best approach to τ-charm physics. Sections 3-5 discuss the initial $\tau^{\pm}$, charm, and J/ψ / ψ' physics goals. The design of the τcF machine and detector is presented in sections 6 and 7, respectively. Finally, we mention the sites where the τ-charm Factory is presently under consideration as a possible construction project.

1 Introduction

Today, particle physics finds itself in the remarkable situation where all established experimental observations can be interpreted within a single theoretical framework - the Standard Model of electroweak interactions and QCD. However, the Standard Model leaves several major questions unanswered, such as why there are three (or more?) families, what is the origin of the observed masses of the fermions and why, for the quarks but apparently not for the leptons, are the weak and mass eigenstates different? The challenge now is to carry out experiments that may shed light on these questions and guide us beyond the current orthodoxy.

Progress during the last few decades has shown that revolutionary advances in our understanding of the laws of nature are made by: a)the birth of new 'elementary' particles, b)the death of old conservation laws, and c)a precise understanding of the symmetries and parameters of the standard theory. With this in mind, we can define the framework for future experiments as follows:

- **Measure fundamental parameters of the Standard Model** e.g. find the missing pieces – H^0, t – and make precise measurements of quantities such as the Kobayashi-Maskawa (KM) matrix elements, the masses of the fundamental constituents, mixing, CP violation, and decays, such as leptonic decays, that are precisely calculable. The aim is both to strengthen the experimental basis underpinning the electroweak interactions and QCD, and also to search for small deviations from the theoretical

expectations.

- **Search for new processes outside the Standard Model** e.g. look for new particles (SUSY, leptoquarks, new scalars, etc.) and for violations of symmetry principles or conservation laws, such as lepton number conservation. New particles can be identified either by direct production or by the subtle effects of virtual propagators on the decays of light particles.

Historically, progress in accelerator-based particle physics has been largely dictated by experiments at the highest energy. However, it is apparent from the above list that fundamental advances can be made – and, indeed, have been made – at lower energies. We anticipate that a greater balance will evolve during the next decade between two *complementary* classes of machine:

1. Supercolliders (energy frontier).

2. Factories (precision/rarity frontier at present energies).

The complementarity of these machines is, in essence, that the supercollider has the greater potential for discovering new particles whereas the factory can focus on previously-discovered particles and measure their properties with unmatched precision.

In addition to a compelling physics case, there are several technical reasons that support this evolutionary viewpoint:

- Most new physics signals at the next generation of supercolliders will be difficult to observe – due either to large backgrounds or small signal rates, or both. Moreover, in the case of hadron supercolliders, the experimental requirements are very challenging and a great deal of R&D is necessary to prepare suitable detectors. Finally, the costs of the next generation supercolliders and their detectors rank them as the most expensive reasearch tools yet seen by the world.

- Several decades of experience since the pioneer machines has opened up the possibility of building factories with extremely high luminosities; increases of up to 100-1000 are feasible. This possibility, combined with advances in detector technology since the initial experiments, indicates the potential exists for major experimental advances at present energies. Furthermore, since the masses of previously-discovered fundamental particles are known, optimized machines and detectors can be built to concentrate on their study. Finally, the cost of a factory, including its detector, can be less than the cost of a general-purpose detector at a *present* supercollider.

In most cases, high-luminosity e^+e^- colliders provide the best factories since the beam energy can be tuned to produce the desired particles under low background conditions. The performance of present and future e^+e^- colliders is illustrated in Figure 1. As discussed in the following section, the threshold region of the particles under study generally provides the optimum experimental conditions. Several particle thresholds have been identified in this energy range – ϕ, τ-charm, bottom, and Z^0 – and each of these regions is currently under consideration for a dedicated particle factory.

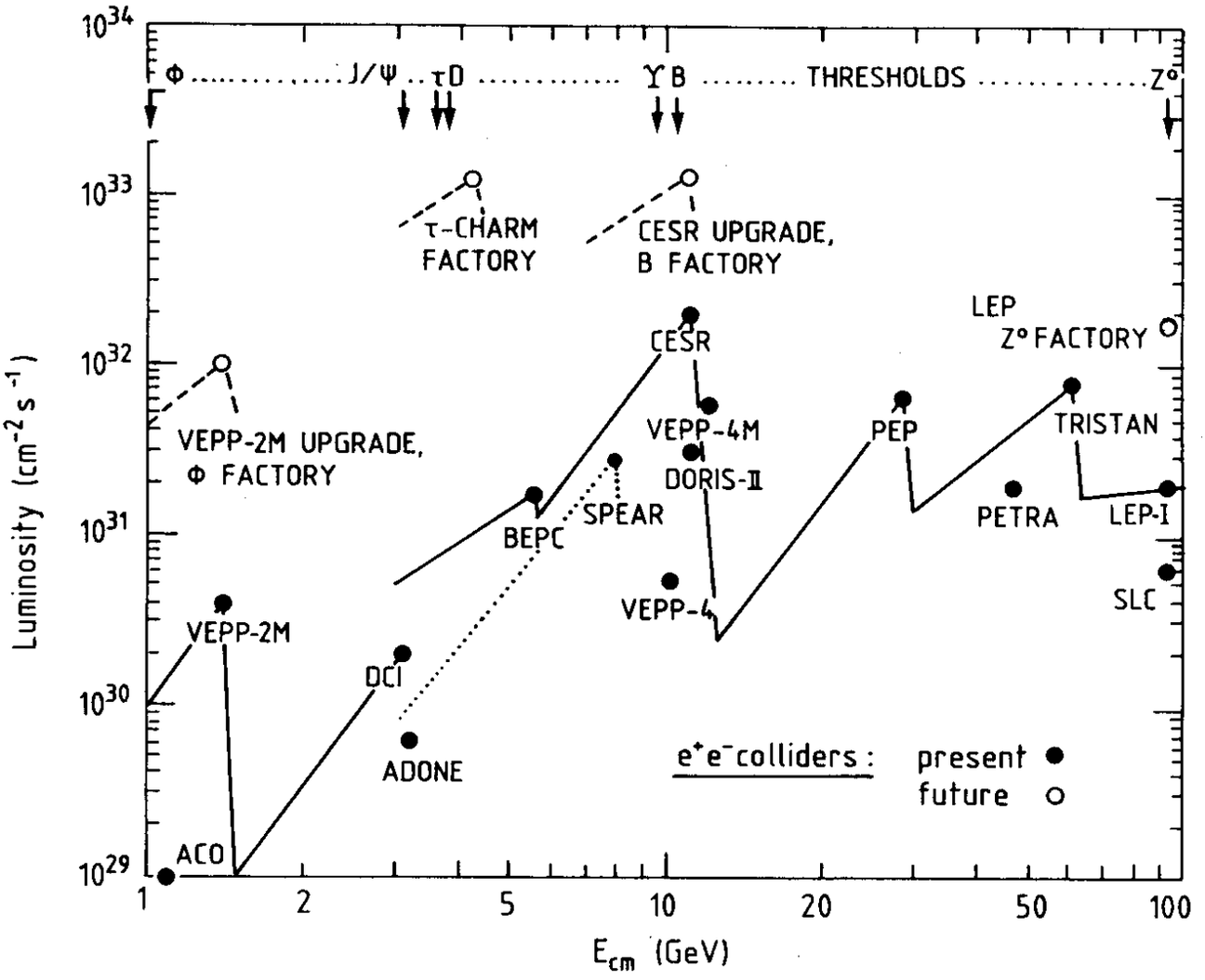

Figure 1: The luminosity of present and future e^+e^- colliders in the energy range $1 \leq E_{cm} \leq 100$ GeV. The solid line represents the present envelope of the maximum luminosity. The dashed lines indicate the design luminosities of future factories. The dotted line shows the current (SPEAR) luminosity in the τ-charm region.

	Luminosity $cm^{-2}\ s^{-1}$	σ ($b\bar{b}$) nb	σ ($c\bar{c}$) nb	σ ($\tau^+\tau^-$) nb
LEP Z^0 Factory	$2\,10^{32}$	5.1	4.0	1.1
B Factory [$\Upsilon(4S)$]	10^{33}	1.0	1.0	0.8
τ-charm Factory	10^{33}	0	[$\psi''(3.77)$] 5.0	[3.57 GeV] 0.5
		0	[4.03 GeV] 15.0	[3.67 GeV] 2.3

Table 1: Luminosities and production cross-sections of e^+e^- collider Factories.

It is quite possible that the primary rôle of *all* future e^+e^- colliders will be factories, rather than tools to search new energy frontiers. This follows from the extreme technological challenges that face TeV e^+e^- linear colliders, in contrast with the feasibility of a 40 TeV hadron collider with present technology. In terms of energy in the 'constituent' frame, the achievable reach of future electron machines has fallen far behind that of proton machines. However the advantage of e^+e^- machines to make precise studies under low-background conditions can be exploited in, for example, a future e^+e^- linear collider factory to study the t quark, *after* its mass has been measured at a proton collider.

2 The best approach to τ-charm physics

In order to make significant progress in τ-charm physics, future data samples must have:

1. high statistics,
2. low backgrounds,
3. reduced systematic biases, and
4. improved detector performance.

The precisions of current measurements are limited by one or more of these aspects. We may illustrate this in the case of $\tau^\pm$ decays. Here, searches for rare decays are generally limited only by statistics, whereas an improved sensitivity to the ν_τ mass requires both more statistics and a reduction of heavy-flavour backgrounds. On the other hand, present measurements of the exclusive one-prong branching ratios are limited by backgrounds, systematics and insufficient detector performance, rather than by statistics.

In the remainder of this section, we discuss in turn how the τ-charm Factory addresses each of these four limitations and why it represents the best approach to τ-charm physics.

2.1 Statistics

The cross-sections for $e^+e^- \to$ *hadrons* and $e^+e^- \to \tau^+\tau^-$ are shown in Figures 2 and 3. These figures illustrate that the maximum $\tau^\pm$ and charm cross sections occur near to threshold. The rate advantage with respect to a B Factory or the LEP Z^0 Factory (Table 1) is $\simeq$ 5–10.

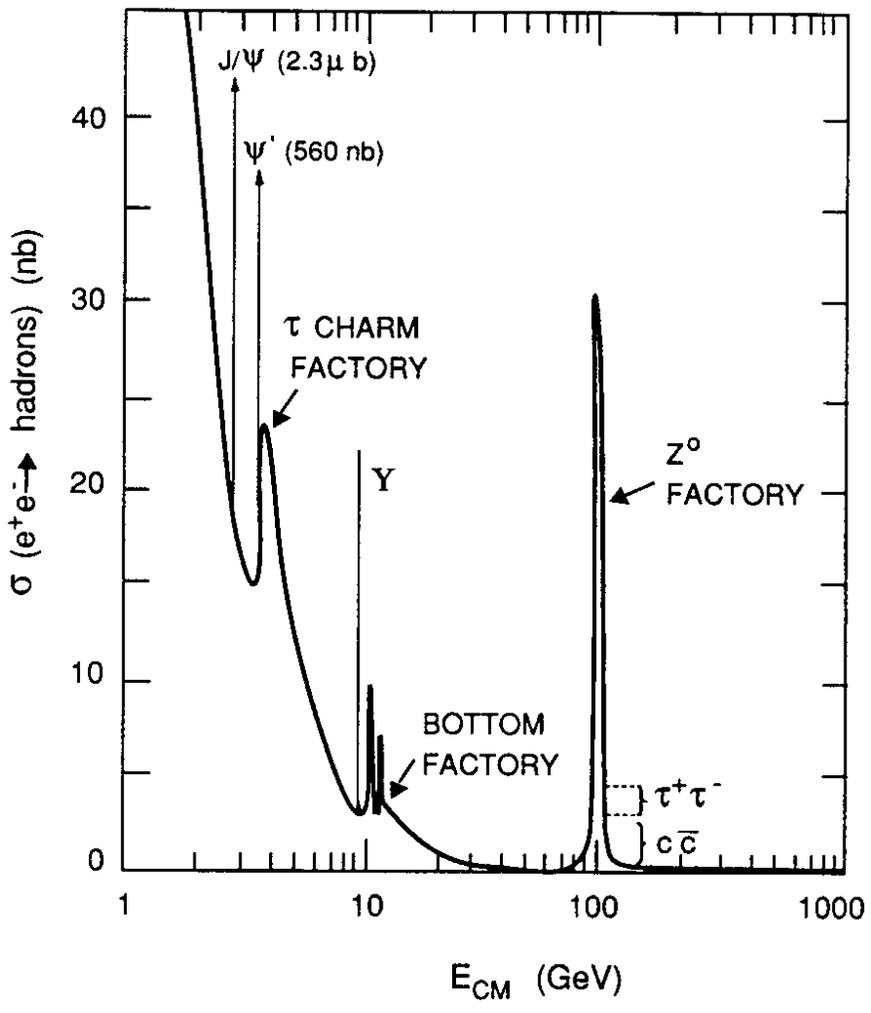

Figure 2: The hadronic cross section, $\sigma(e^+e^- \rightarrow hadrons)$, in the range $1 \leq E_{cm} \leq 1000$ GeV.

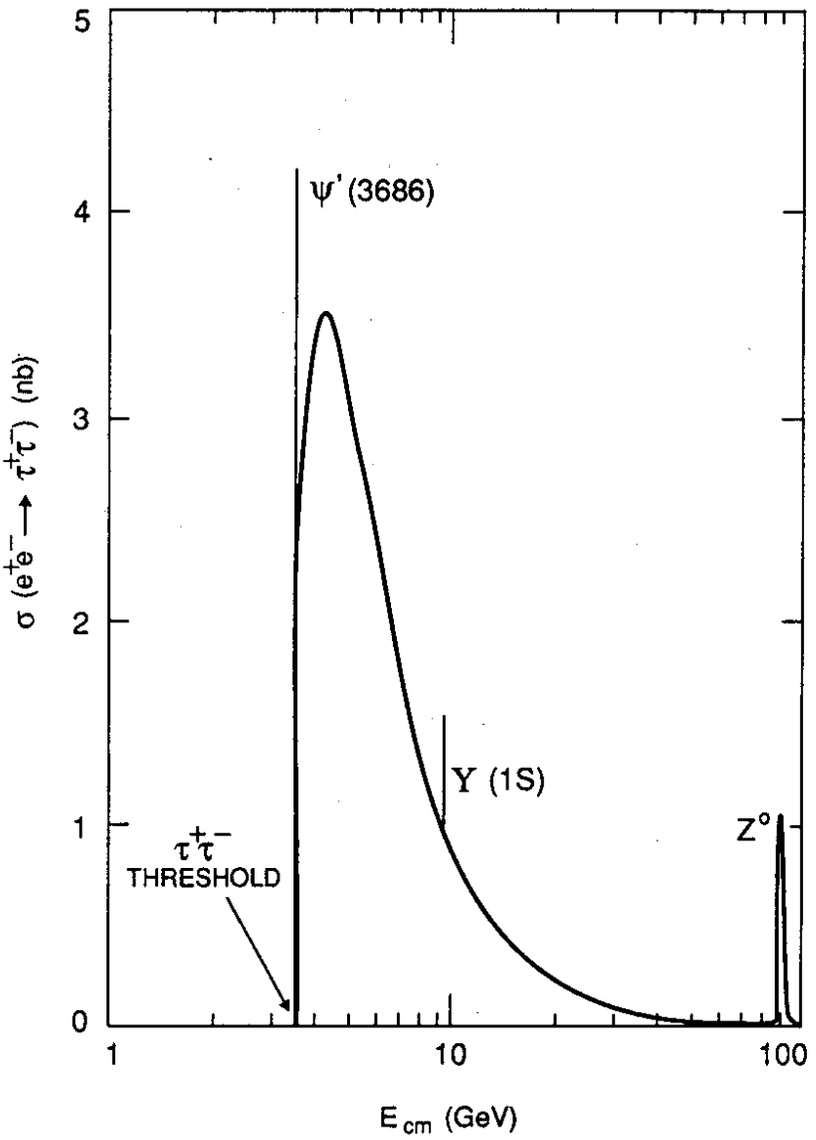

Figure 3: The $\tau^+\tau^-$ cross section, $\sigma(e^+e^- \to \tau^+\tau^-)$, in the range $2\,m_\tau \leq E_{cm} \leq 100$ GeV.

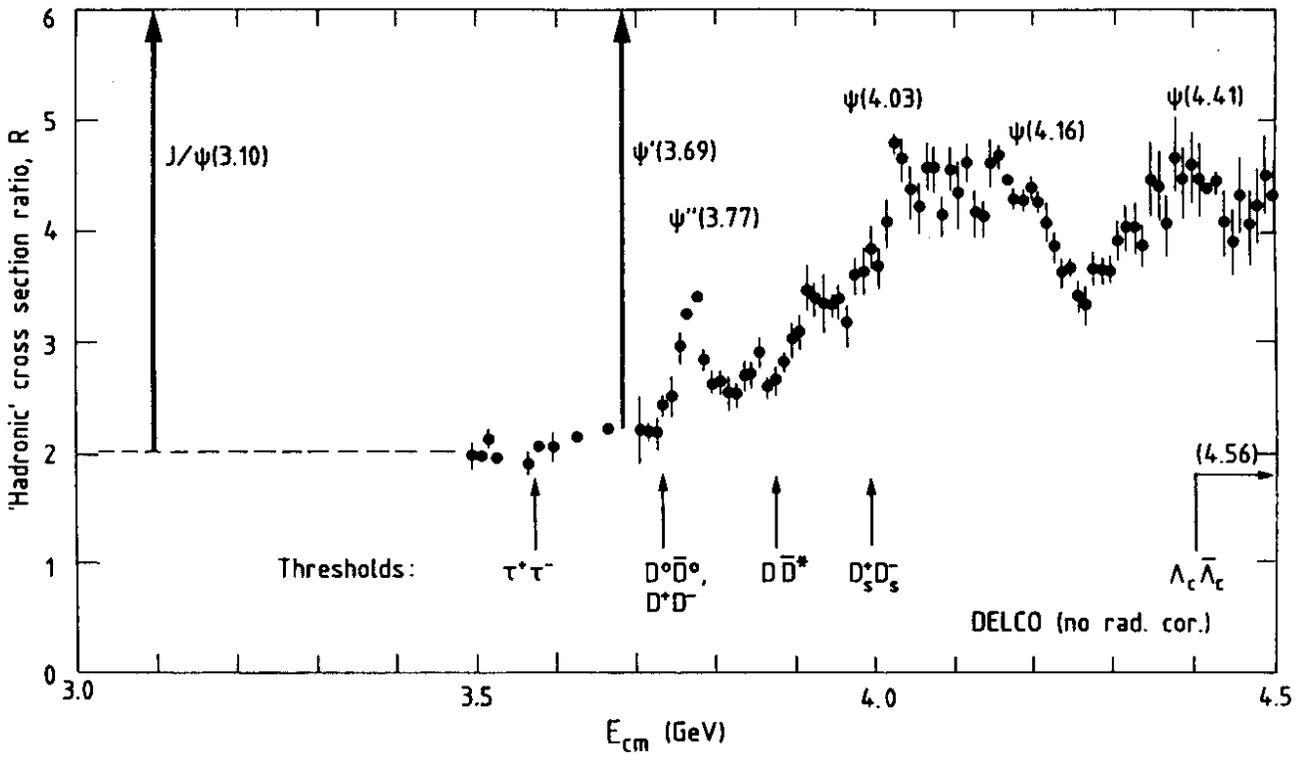

Figure 4: The energy range of the τ-charm Factory . The ratio $R = \sigma(e^+e^- \rightarrow$ 'hadrons') / $\sigma(e^+e^- \rightarrow \mu^+\mu^-)$, where 'hadrons' include both $q\bar{q}$ and $\tau^+\tau^-$ events. The data are from DELCO at SPEAR.

In the case of fixed-target charm studies, future experiments such as E791 plan to obtain an order-of-magnitude higher statistics than the pioneer experiment E691. This will provide approximately 3 10^4 reconstructed events for decays such as $D^0 \rightarrow K^-\pi^+$ or $D^+ \rightarrow K^-\pi^+\pi^+$. For comparison, the τcF will obtain $\simeq$ 2 10^6 events per year in each of these decay channels.

2.2 Backgrounds

The τcF energy range (Figure 4) includes several unique operating points for τ-charm studies which have backgrounds that are both exceptionally low *and* internally calibrated by small shifts in E_{cm}. These energies (Table 2) are as follows:

- **$J/\psi(3.10)$ and $\psi'(3.69)$.**
- **$\tau^{\pm}$ studies:**
  - **3.55 GeV.** This energy, which is just below $\tau^+\tau^-$ threshold, provides a direct measurement of all non-$\tau^{\pm}$ backgrounds: hadronic ($u\bar{u}$, $d\bar{d}$ and $s\bar{s}$), two-photon, QED and beam-gas.
  - **3.57 GeV.** A recent calculation[2] has shown that the $\tau^+\tau^-$ cross section has a finite value (0.223 nb) precisely at threshold, due to a Coulomb interaction

Particles	E_{cm} GeV	# events per year
J/ψ	3.10	10^{10}
ψ'	3.69	$6\,10^9$
$\tau^+\tau^-$	3.57	$4\,10^6$
$\tau^+\tau^-$	3.67	$2\,10^7$
$\tau^+\tau^-$	4.25	$4\,10^7$
D^+D^-	$\psi''(3.77)$	$2\,10^7$
$D^\circ\bar{D}^\circ$	$\psi''(3.77)$	$3\,10^7$
$D_s^+D_s^-$	4.03	$7\,10^6$
$D_s^\pm D_s^{\star\mp}$	4.14	10^7

Table 2: Operating points and data samples at the τ-charm Factory. A peak luminosity $10^{33}\,\mathrm{cm}^{-2}\mathrm{s}^{-1}$ and a peak integrated luminosity $10^4\ \mathrm{pb}^{-1}$ per year, at $E_{beam} = 2.0$ GeV, are assumed.

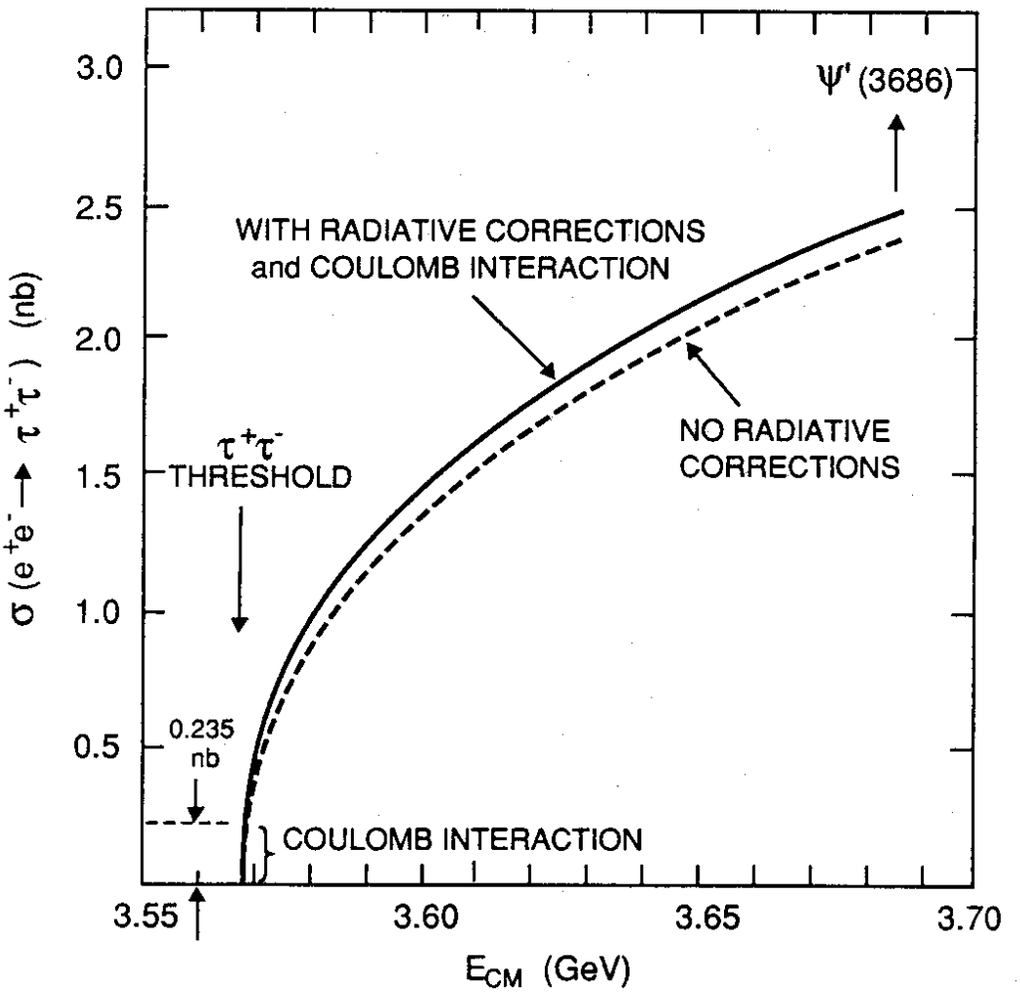

Figure 5: The $\tau^+\tau^-$ cross section $\sigma(e^+e^- \to \tau^+\tau^-)$ near to threshold[2].

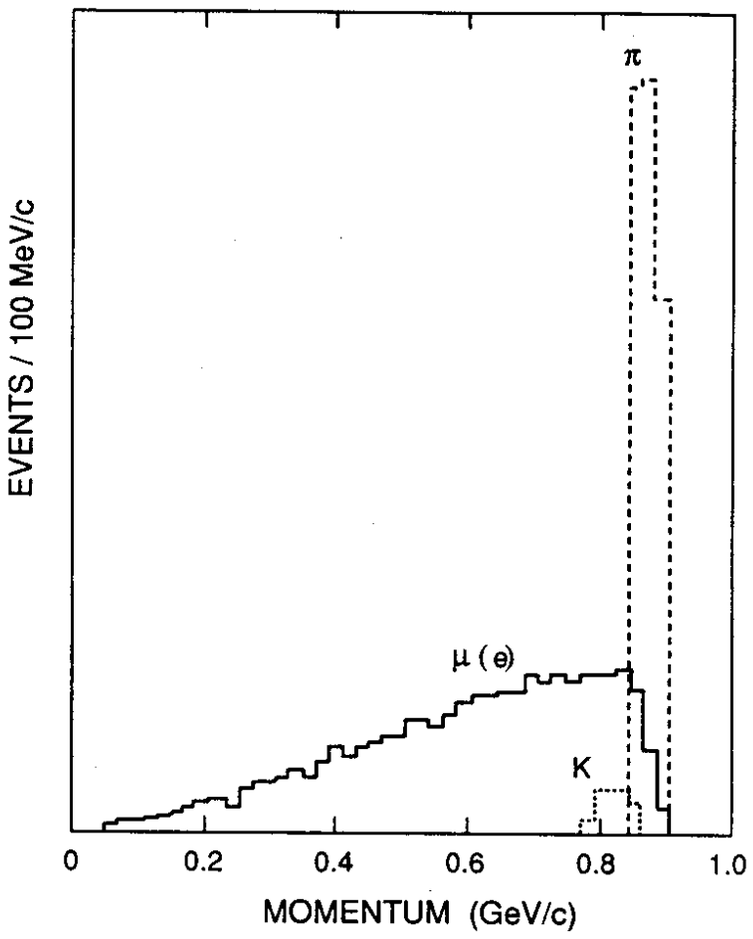

Figure 6: The momentum spectra from single-charged-particle $\tau^{\pm}$ decays at $E_{beam} = 1.785$ GeV.

between the τ^+ and τ^- (Figure 5). When the beam energy is set to $m_\tau + \sigma_\epsilon$ (the beam energy spread, which is 1.0 MeV at this energy) the $\tau^+\tau^-$ cross section is 0.47 nb. This introduces an important new operating point for $\tau^{\pm}$ physics, with the following features:

* Monochromatic two-body decays e.g. $\pi\nu_\tau$, $K\nu_\tau$ and $\rho\nu_\tau$. The $\tau^{\pm}$ velocity is simply determined by the beam energy spread, i.e. $\beta_\tau = 0.024$. The momentum spread of the two-body decays is therefore only $\pm$ 2.4%. This implies that the $\pi\nu_\tau$ and $K\nu_\tau$ decays are *kinematically* separated ($\bar{p}_\pi = 887$ MeV/c and $\bar{p}_K = 824$ MeV/c) and both are distinct from the $\mu\nu_\mu\nu_\tau$ decay spectrum (Figure 6). The one-prong decays can therefore be measured with high precision. Furthermore the signature of a monochromatic $\pi + E_{miss}$ (the 'missing' energy in the event, due to ν's) is sufficiently distinct to provide a clean single-tag of $\tau^+\tau^-$ events[3].
* Capability to make a precise measurement of the $\tau^{\pm}$ mass. It should be possible to measure the $\tau^{\pm}$ mass to 10% of the beam energy spread, i.e. 0.1 MeV/c^2. This may be reduced by approximately a factor of 5 if monochromator optics

can be successfully implemented[4,5].

* Absence of large radiative corrections to the kinematics of the $\tau^+\tau^-$ events. This applies in general to the $\tau^+\tau^-$ threshold region and is a significant advantage in certain experiments, such as the precise measurement of the $\tau \to e\nu_e\nu_\tau$ electron spectrum.

- **3.67 GeV**. This energy provides the highest $\tau^+\tau^-$ cross section below the $\psi'(3.69)$ and $D\bar{D}$ threshold (3.73 GeV), where $\tau^\pm$ decay is the *only* source of prompt single leptons. The $\tau^\pm$ cross section is large: 65% of its maximum value in the continuum. The $\tau^\pm$ velocity is small ($\beta_\tau = 0.23$) and so the effects of Lorentz smearing on momentum distributions etc. are also small.
- **4.25 GeV**. At this energy, the $\tau^\pm$ continuum rate has its maximum value, coinciding with a *minimum* in the charm cross section. The advantages here are the high rate and finite $\beta_\tau = 0.54$, which results in large polarization correlations in $\tau^+\tau^-$ decays. (These correlations vanish as $\beta_\tau \to 0$.) The presence of charm backgrounds, however, limits the range of experiments that are feasible.

- **Charm studies:**
  - $\psi''(3.77)$. This energy provides pure $D^o\bar{D}^o$ and D^+D^- final states, without contamination from other charmed particles or from jet fragments, thereby allowing studies of *tagged* D^0 and $D^\pm$ decays.
  - **4.03 GeV**. This energy gives the highest charm cross section in e^+e^- annihilation and is suitable for tagged $D_s^\pm$ studies.
  - **4.14 GeV**. This is a second identified energy for $D_s^\pm$ studies, via $D_s^\pm D_s^{*\mp}$ events. It is possible that there are better choices of beam energy for $D_s^\pm$ studies than these, since present measurements of the hadronic cross section and charmed particle yields in this region are poor. In this remains the case, an early part of the τcF physics program will be to carry out a precise scan of the hadronic cross section over the charm threshold region.

A key experimental feature of the τ-charm threshold region is the ability to *tag* a particle, whose decays can then be studied without bias, with exceptionally low backgrounds and with absolute flux normalization. This technique has been used extensively at $\psi''(3.77)$, e.g. to provide unique measurements of D^0 and $D^\pm$ absolute branching ratios. In the case of $D_s^\pm$, however, absolute branching ratio measurements have not yet been possible since the statistics are too poor; not a single example exists of a double-tagged $D_s^+D_s^-$ event. The τ-charm Factory will collect the following single-tagged samples per year: $7\ 10^6$ $D^o\bar{D}^o$ events [$\psi''(3.77)$], $4\ 10^6$ D^+D^- events [$\psi''(3.77)$], and 10^6 $D_s^\pm D_s^{*\mp}$ events [4.14 GeV].

Furthermore, for the first time at any machine, we expect to be able to single-tag $\tau^+\tau^-$ events. All previous $\tau^\pm$ measurements have employed global event selection criteria that impose restrictions on *both* $\tau^\pm$ decays in each event. In this case, the observed number of events is,

$$N_{ij} = 2\, N_{\tau\bar{\tau}}\, B_i\, B_j\, \epsilon_{ij}$$

where $N_{\tau\bar{\tau}}$ is the number of $\tau^+\tau^-$ events, B_i is the branching ratio to a final state i and ϵ_{ij} is the detection efficiency for the combined final state ij. This event selection allows *relative* branching ratios to be determined without knowledge of $N_{\tau\bar{\tau}}$. However, *absolute* branching ratios depend on a determination of $N_{\tau\bar{\tau}} = \sigma_{\tau\bar{\tau}} \int L\, dt$. This requires a calculation of $\sigma_{\tau\bar{\tau}}$ and a measurement of luminosity, which limits the accuracy to a few percent.

A better technique is to tag the $\tau^+\tau^-$ event by means of a *single* $\tau^\pm$ decay, leaving the second $\tau^\pm$ to decay in an unbiased way. This provides a parent $\tau^\pm$ data sample with zero normalization uncertainty and also ensures that the remaining particles in the event must all originate from the same parent $\tau^\pm$. The observed number of events in which the second $\tau^\pm$ decays to a state i is simply,

$$N_i = N_\tau\, B_i\, \epsilon_i$$

where N_τ is the number of events in the single-tagged sample.

Of course, the application of single-tagging requires a signature from a single $\tau^\pm$ decay that is very clean. With the unique capability of the τ-charm Factory to produce $\tau^+\tau^-$ events near threshold and without contamination from heavy flavour decays, several signatures fulfill this requirement, as follows:

1. $e + E_{miss}$
2. $\mu + E_{miss}$
3. Monochromatic $\pi + E_{miss}$ (at 3.57 GeV). This may also be extended to include a monochromatic ρ or $a_1(1260)$.

For example, with the signature $e + E_{miss}$, which has an efficiency of $\simeq 0.22$ for $\tau^+\tau^-$ events, the τcF detector provides a rejection factor $3\,10^{-5}$ for hadronic events below charm threshold[6]. This results in background levels $\leq 10^{-3}$ at $E_{cm} = 3.67$ GeV and $\leq 5\,10^{-3}$ at $E_{cm} = 3.57$ GeV. This signature alone will provide yearly tagged $\tau^\pm$ samples of $4\,10^6$ events at 3.67 GeV, or $0.9\,10^6$ events at 3.57 GeV.

In single-tagged events, in view of the excellent rejection of events from background sources, the small residual background is almost entirely from decays of the $\tau^\pm$ or D under study, in which particles are either misidentified or undetected. The key to maintaining these backgrounds at a low level is good-quality particle identification, high efficiency and high resolution in the τcF detector.

At a B factory it is not possible to single-tag either $D^\pm$ or $D_s^\pm$ (due to the lack of pure $D\bar{D}$ final states) or $\tau^\pm$ (due to the presence of heavy-flavour backgrounds). The one exception is D^0 tagging via the soft π^+ in $D^{*+} \rightarrow D^0\, \pi^+$. However, this D^0 tag, which is also the only technique available in fixed-target studies, generally has a sizeable background (an example is shown in Figure 15).

The absence of single-tagged τ-charm data samples results in higher backgrounds at other accelerators. At energies far from threshold, the backgrounds must in general be calculated by Monte Carlo, whereas they are experimentally measured at the τ-charm Factory. Furthermore, at a B factory, since the heavy flavoured particles τ, D and B are all produced at a given beam energy (Table 1), each may contribute backgrounds to the others. For example, in the case of $D^o\bar{D}^o$ mixing, the presence of a large 100% mixed

$B^o\bar{B}^o$ background would swamp the diminutive ($\leq 10^{-4}$) signal. A further example is the multi-lepton signals that are used to detect mixing and rare decays; these suffer additional backgrounds from B semileptonic cascade events.

2.3 Systematic biases

In addition to reducing the backgrounds, tagging allows τ or D decays to be studied with the least systematic biases. In a tagged event, *all* the remaining particles come from a single parent τ or D, and no restrictions are imposed on its decay topology. With single-tagging, certain experiments – such as $D^+ \rightarrow \mu^+\nu_\mu$, $D_s^+ \rightarrow \tau^+\nu_\tau$, or $D^+ \rightarrow \pi^+\nu\bar{\nu}$ – are unique to the τ-charm Factory. Finally, as discussed above, tagging allows precise determination of branching ratios, since there is zero normalization uncertainty.

Further limitations associated with fixed-target charm studies are the exclusion of 0-prong and 1-prong decays, as well as difficulties in handling decays involving neutrals (since neutral particles cannot be directly associated with the charm decay vertex).

2.4 Detector performance

The mass resolutions in the τcF are typically 1-5 MeV/c^2 due to the favourable kinematic conditions: precise E_{cm} constraint, small radiative smearing, exclusive production (and therefore presence of additional kinematic constraints) and low-energy final-state particles. Furthermore, the detection inefficiency caused by charged and neutral pileup is minimized at τcF energies. Another advantage of operating close to τ-charm threshold is that the kinematic limit of particles from $\tau^\pm$ and D decays is $\simeq$ 1 GeV/c and so the identification of π, K and p is relatively easy using a combination of ToF and dE/dx.

In contrast, the kinematic range of the secondary particles at a B Factory extends up to 5 GeV/c. In consequence, particle identification is more difficult and mass resolutions are worse. The experiment to measure the ν_τ mass, from the end-point of the $\tau \rightarrow 5\pi^\pm\nu_\tau$ spectrum, is particularly sensitive to mass resolution; calculations[7] show a factor 3 poorer limit at a B factory due to this aspect alone. [Further limitations include the reduced statistics and the contribution of charm backgrounds to the small signal from $\tau \rightarrow 5\pi^\pm\nu_\tau$ (branching ratio 6 10^{-4}).]

In summary, while there is certainly some overlap with other experiments — fixed-target experiments, the LEP Z^0 Factory or a B factory — the τ-charm Factory, with its statistical superiority, unique operating points, exceptionally low backgrounds and lack of systematic biases, represents by far the best laboratory to explore τ-charm physics.

3 $\tau^\pm$ physics

3.1 ν_τ and $\tau^\pm$ mass measurements

The possibility of non-zero neutrino masses is of central importance to physics. Finite neutrino masses would profoundly affect the Standard Model – allowing mixing and os-

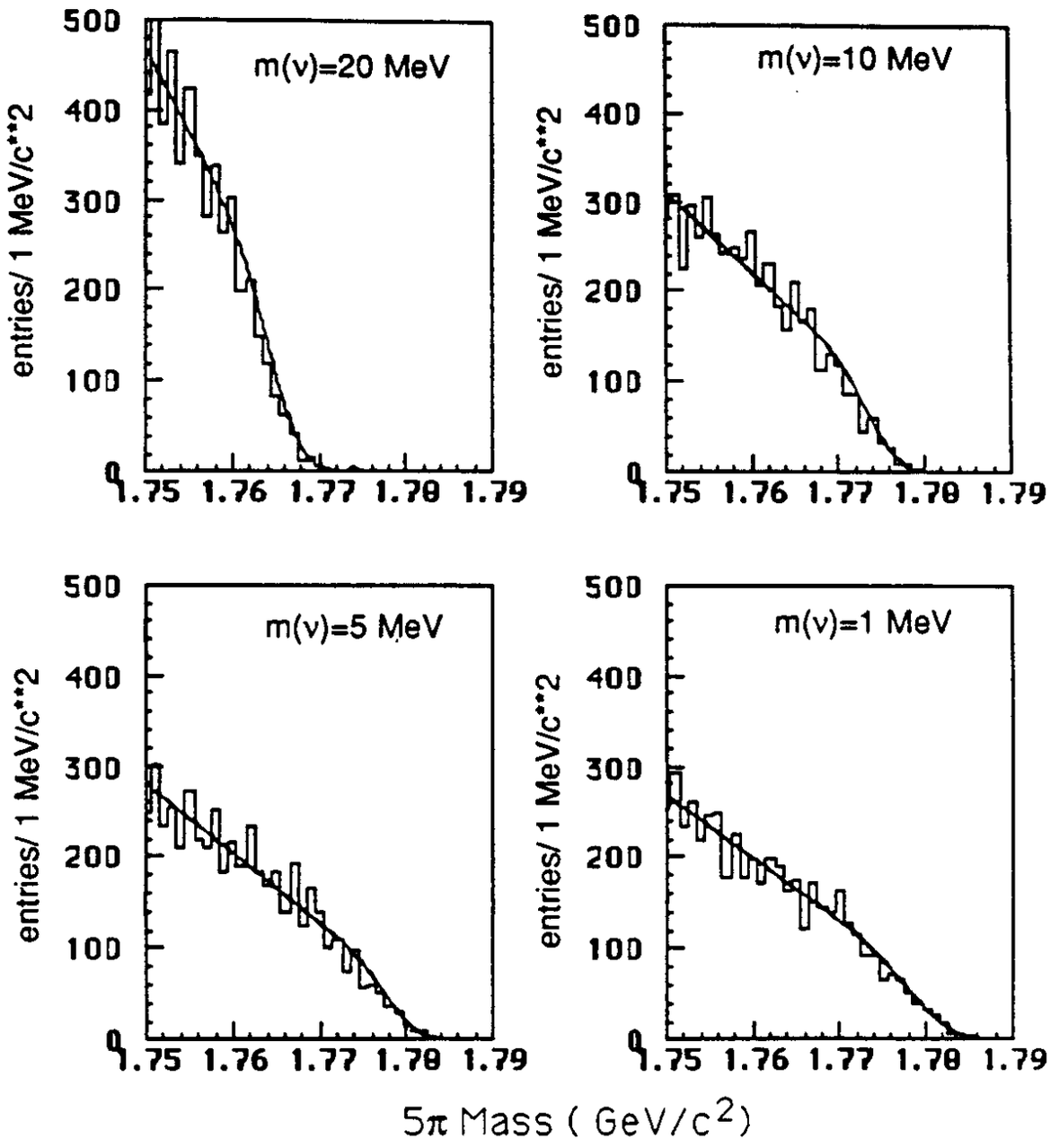

Figure 7: The endpoint spectra for the $5\pi^{\pm}$ invariant mass in the decay $\tau^{\pm} \rightarrow 5\pi^{\pm}\,\nu_{\tau}$. Several values of $m_{\nu_{\tau}}$ are assumed, as indicated. The distributions come from a Monte Carlo data sample of $5\,10^{7}$ $\tau^{+}\tau^{-}$ events[7].

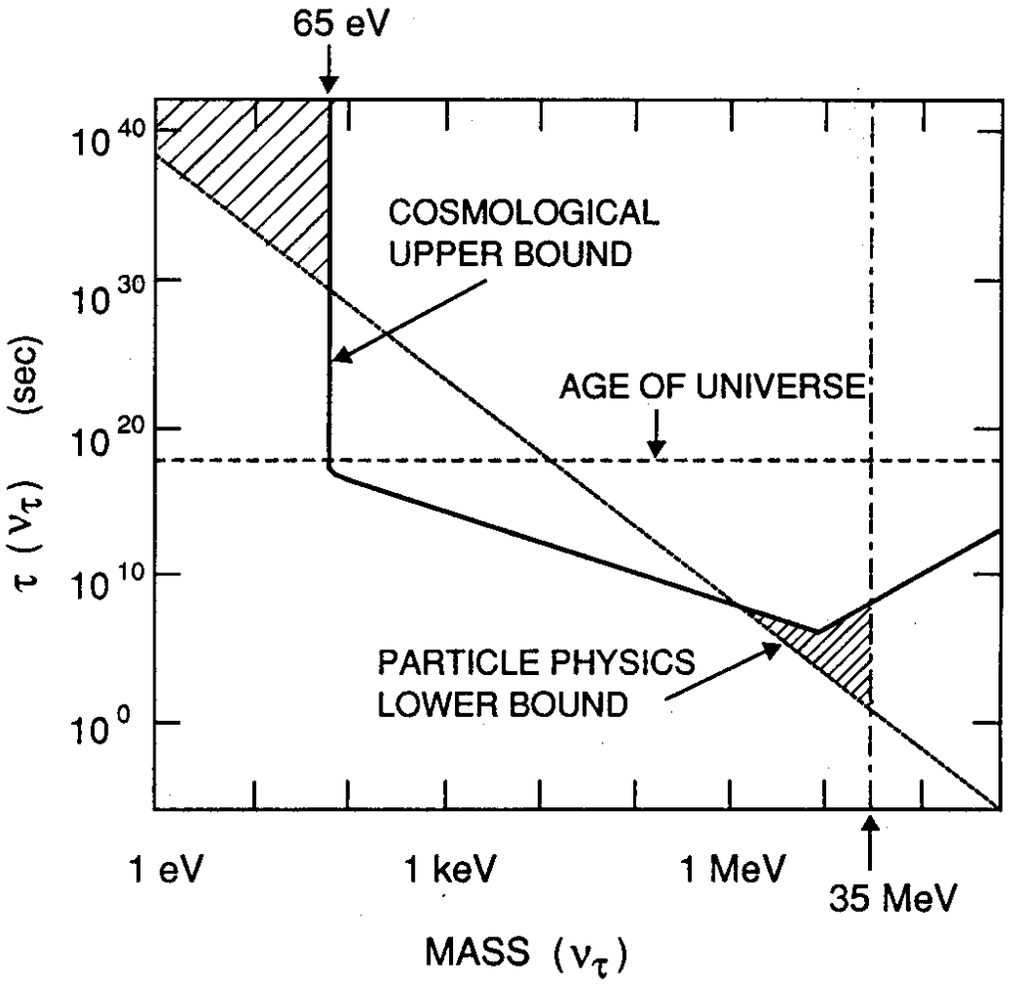

Figure 8: The mass and lifetime of ν_τ[8]. The shaded regions correspond to the allowed values from a combination of particle physics and cosmological constraints. Within these assumptions, the lowest possible mass of an unstable ν_τ is $\simeq$ 1 MeV/c^2.

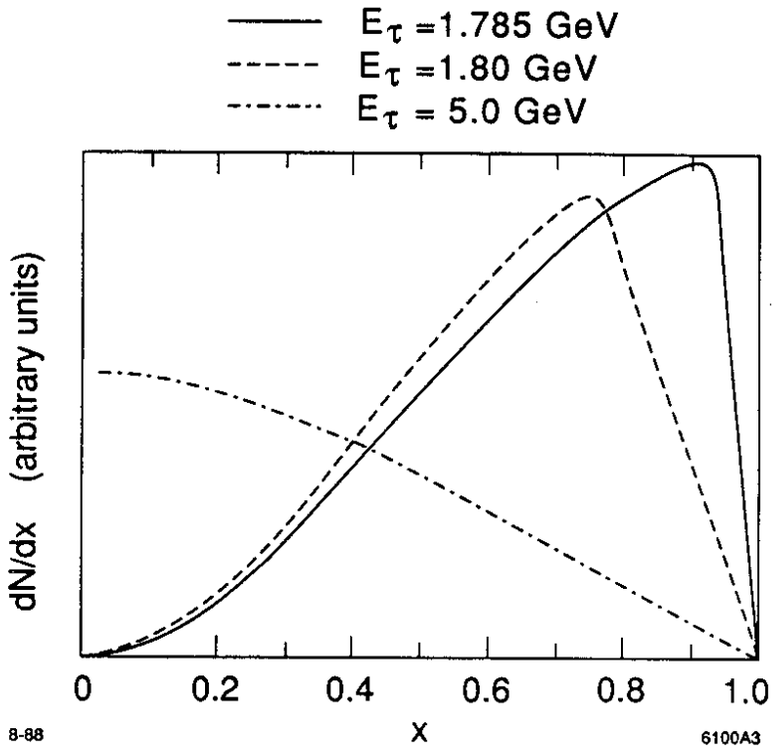

Figure 9: The e/μ energy spectrum from $\tau^{\pm}$ decay (V-A) at several different beam energies.

cillations between lepton families – and also provide answers to two of the major puzzles of cosmological physics: the deficiency of solar neutrinos and the composition of the dark matter of the universe.

The ν_τ mass is investigated by measuring the end-point of the $5\pi^{\pm}$ mass spectrum in $\tau^{\pm} \rightarrow 5\pi^{\pm}\,\nu_\tau$, and the end-point of the $K^-K^+\pi^{\pm}$ mass spectrum in $\tau^{\pm} \rightarrow K^-K^+\pi^{\pm}\nu_\tau$. With a one-year sample of $\tau^{\pm} \rightarrow 5\pi^{\pm}\,\nu_\tau$ events, the upper limit (95% CL) to the ν_τ mass is 3 MeV/c^2 (Figure 7[7]). Including other channels and further statistics, the limiting sensitivity will reach 1 MeV/c^2. These experiments require the τ mass be known with an accuracy $\leq$0.2 MeV/c^2, a measurement that can only be made at the τcF. This is an especially important value of m_{ν_τ} to reach since it represents the lower limit for an unstable ν_τ that is allowed by combined cosmological and particle physics constraints; below this value, the combined results indicate $m_{\nu_\tau} \leq 65$ eV/c^2 (Figure 8[8]). Finally, we point out that it is widely expected that massive ν's would follow the same mass hierarchy as the charged leptons and, in certain models such as the 'see-saw' model[8], $m_{\nu_l} \propto m_l^2$, in which case a sensitivity of 1 MeV/c^2 for m_{ν_τ} is equivalent to 0.1 eV/c^2 for m_{ν_e}.

3.2 e spectrum in $\tau \rightarrow e\nu_e\nu_\tau$

This involves a precise measurement of the decay parameters - ρ, η, ξ and δ - and a sensitive search for deviations from the V-A interaction due to anomalous decays or currents which may be hidden under the standard $\tau \rightarrow e\nu_e\nu_\tau$ spectrum. For example, perhaps there is a *second*, massive, τ neutrino ($\tau \rightarrow e\nu_e N_\tau$), a lepton-number-violating neutral particle

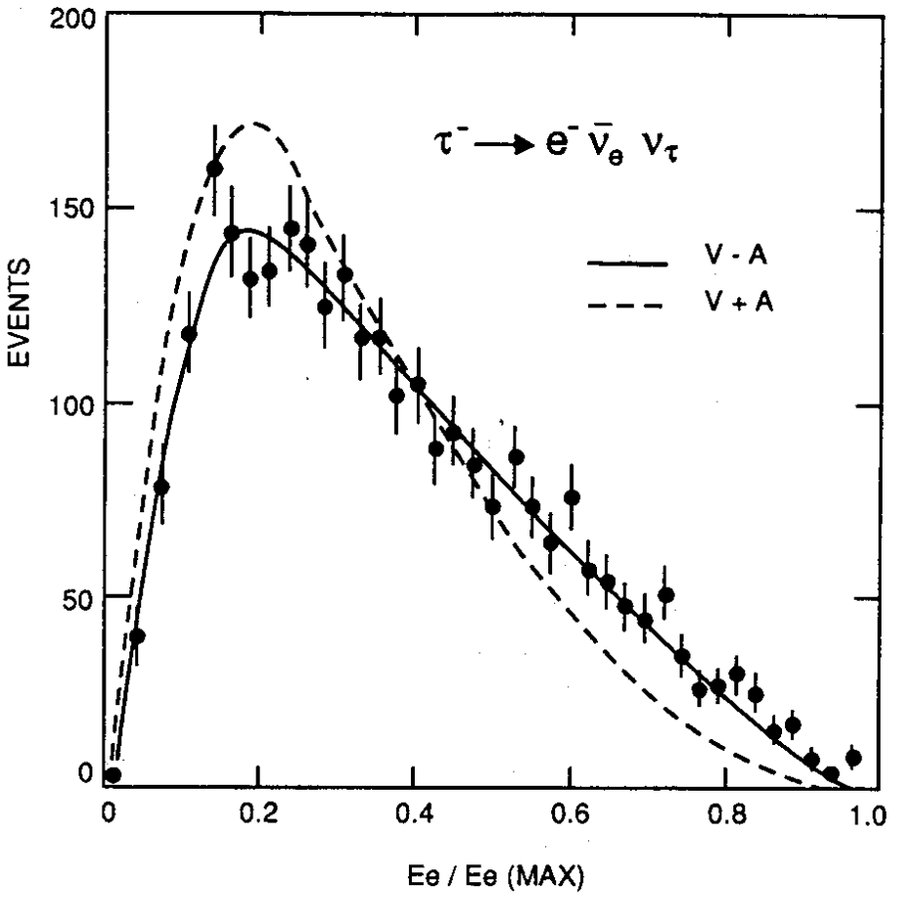

Figure 10: The ARGUS measurement of the electron energy spectrum from $\tau^{\pm}$ decays at $E_b \simeq 5$ GeV.

($\tau \rightarrow eX^0$), or a charged Higgs ($\tau^- \rightarrow (H^-\nu_\tau) \rightarrow e^-\bar{\nu}_e\nu_\tau$)? Current data cannot exclude the possibility of an anomalous decay such as $\tau \rightarrow e\nu_e N_\tau$, even at a branching ratio as big as 1%.

The ρ and η parameters are determined by fitting the electron energy spectrum, ideally close to threshold where the effects of the Lorentz boost are small (Figure 9). The ξ and δ parameters are determined by measuring the spin-spin correlations at $E_{cm} = 4.25$ GeV. The only decay parameter measured so far is the Michel parameter ρ, with a world-average value 0.74±0.05. At present, the most precise single measurement is from ARGUS, which finds $\rho = 0.77 \pm 0.09$ (Figure 10[9]). The τcF will measure the τ leptonic decay parameters to an accuracy comparable with those measured for μ decays; the expected errors[7] are as follows: ρ (±0.003), η (±0.2), ξ (±0.02), and δ (±0.02).

3.3 Precise branching ratio measurements

The decay rates of many $\tau^{\pm}$ decay modes can be rigorously calculated, and so precise measurements of the branching ratios provide excellent tests of the Standard Model. Table 3 shows that the precision of the present experimental values falls far short of testing the

Ratio	No electroweak corrections	With electroweak corrections	Experimental value
$\mu^-\bar{\nu}_\mu\nu_\tau/e^-\bar{\nu}_e\nu_\tau$	0.973	0.973	1.02 $\pm$0.03
$\pi^-\nu_\tau/e^-\bar{\nu}_e\nu_\tau$	0.607	0.601	0.62 $\pm$0.04
$K^-\nu_\tau/e^-\bar{\nu}_e\nu_\tau$	0.0395	0.0399	0.038$\pm$0.011

Table 3: Standard Model predictions and experimental values for some $\tau \rightarrow 1-prong$ relative branching ratios[3].

theory. At the τ-charm Factory, these branching ratios will be measured to an accuracy $\simeq$ 0.5-1.0% that is sufficiently sensitive to probe the electroweak corrections, or new physics of comparable strength. For example, a charged Higgs could increase, by a few percent, the $\mu\nu_\mu\nu_\tau$ branching ratio relative to $e\nu_e\nu_\tau$[2]. Effects of a charged Higgs could be seen elsewhere in $\tau^\pm$ decays, such as the angular distributions in $\tau^- \rightarrow \pi^-\pi^0\nu_\tau$[10].

The discrepancy[11] between the inclusive $\tau \rightarrow 1-prong$ branching ratio (0.866$\pm$0.003) and the sum of the exclusive 1-prong decays ($\leq .805 \pm 0.019$) – the so-called 'one prong problem' – remains an open question for the Standard Model. It is likely that the resolution of this discrepancy – be it experimental errors or new physics – will require an experiment with the special characteristics of the τcF. Decay modes involving neutral particles are particularly poorly measured at present. The τcF will substantially improve knowledge of such decays, where it has the notable advantage of lack of neutral pileup. The sensitivity to neutral decay modes will extend to an observation of the rare (br 1.5 10^{-5}) decay $\tau^- \rightarrow \pi^-\eta\nu_\tau$[12].

Finally, we note that $\tau^\pm$ decays can be used to explore light quark spectroscopy ($m \leq m_\tau$) produced by the charged weak current in $\tau^- \rightarrow \nu_\tau W_v^-$, $W_v^- \rightarrow \bar{u}d/\bar{u}s$. As in e^+e^- annihilation, this may prove to be far cleaner than hadronic production for creating certain mesons.

3.4 Determination of α_s and $\Lambda_{\overline{MS}}$

Determinations of α_s in e^+e^- processes have generally fallen into two categories: the method is clean but the experimental accuracy is poor, or the experimental accuracy is good but the method is beset with (e.g. fragmentation) uncertainties. Pich[13] argues that τ decays provide an ideal way to determine α_s, by measuring the ratio

$$R_\tau = \Gamma(\tau \rightarrow \nu_\tau\ hadrons)/\Gamma(\tau \rightarrow \nu_\tau\nu_e e)$$

This has been calculated to third order in α_s/π, and shows a large third order coefficient, whereas the non-perturbative effects and radiative corrections are found to be small. The large third-order coefficient implies good sensitivity to $\Lambda_{\overline{MS}}$, although it raises questions concerning the convergence of the perturbative expansion. The predicted values of R_τ are shown in Table 4. The experimental values (Table 5) are not consistent with each other, reflecting the '1 prong problem' and other discrepancies in the present measurements. Using the average of the measurements in Table 5 gives $\Lambda_{\overline{MS}} \simeq 150\pm30$ MeV. A comparison

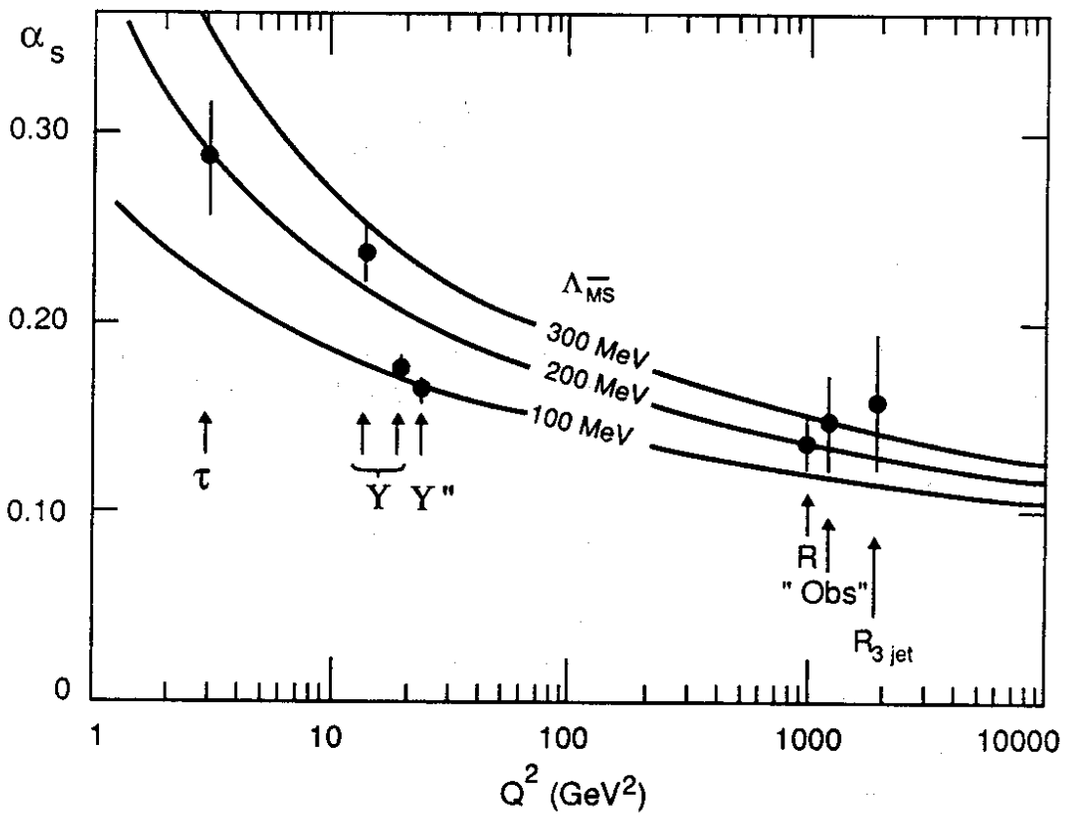

Figure 11: A comparison of α_s measurements in e^+e^- annihilation that are largely independent of fragmentation models[14]. In these data $R_\tau = 3.49 \pm 0.09$, as determined from a τ electronic branching ratio $B_e = 0.183 \pm 0.003$.

$\Lambda_{\overline{MS}}$ (MeV)	R_τ(theory)
100	3.35 ± 0.06
200	3.67 ± 0.01
300	4.02 ± 0.01

Table 4: Standard Model predictions for $R_\tau = \Gamma(\tau \to \nu_\tau\ hadrons)/\Gamma(\tau \to \nu_\tau \nu_e e)$ [13].

Method	R_τ(experiment)
Exclusive modes	3.22 ± 0.10
τ lifetime	3.27 ± 0.16
br$(\tau^- \to \mu^- \bar{\nu}_\mu \nu_\tau)$	3.49 ± 0.12
br$(\tau^- \to e^- \bar{\nu}_e \nu_\tau)$	3.74 ± 0.13
Average	3.53 ± 0.08

Table 5: Experimental values for $R_\tau = \Gamma(\tau \to \nu_\tau\ hadrons)/\Gamma(\tau \to \nu_\tau \nu_e e)$, obtained by several different methods[13].

of this technique with others in e^+e^- annihilation is shown in Figure 11[14], illustrating the improved sensitivity to $\Lambda_{\overline{MS}}$ at the low Q^2 corresponding to τ decays.

3.5 Rare τ decays

These modes involve neutrino-less decays such as $\tau^- \to l^-\gamma, l^-\mu^+\mu^-, l^-e^+e^-, h^0l^-, h^-e^-\mu^+$ etc., where $l = e, \mu$ and $h = hadron(s)$. The experimental limits on most of these decays are limited only by statistics, since backgrounds are negligible. The τcF will be sensitive to branching ratios near 10^{-7} – an improvement by a factor 100-1000 compared with present limits. It is likely[15,16] that rare τ decays will be much more sensitive to new physics than the equivalent rare μ decays since $m_\tau \gg m_e, m_\mu$ and, in addition, there is a broad range of kinematically-allowed channels.

4 Charm physics

4.1 KM matrix elements V_{cs}, V_{cd}

These fundamental parameters of the Standard Model are poorly measured at present (Table 6). The semileptonic decays of D mesons (Figure 12) provide the most direct measurements of V_{cs} and V_{cd}. As examples,

$$\Gamma(D \to Ke\nu_e) \propto | f_+^K(t^2) |^2 \ | V_{cs} |^2,$$

$$\Gamma(D \to \pi e\nu_e) \propto | f_+^\pi(t^2) |^2 \ | V_{cd} |^2,$$

where $f_+^{\pi,K}(t^2)$ are form factors. Using tagged events at $\psi''(3.77)$, these decays can be identified in fully constrained events with a single missing ν. Although the signature is

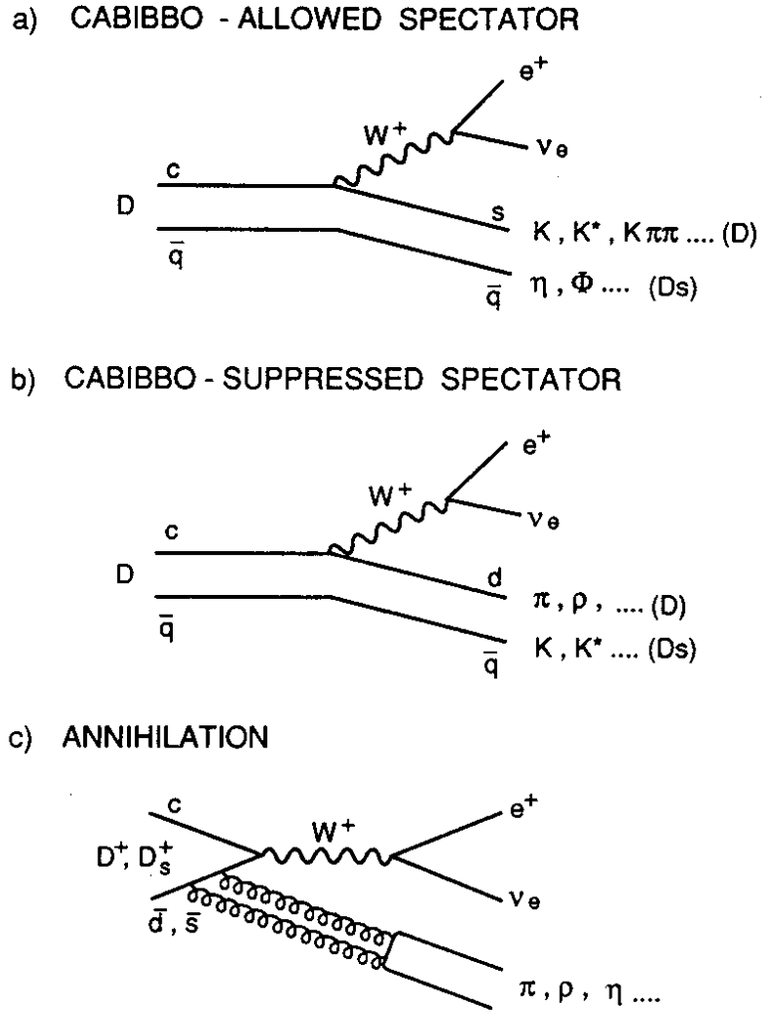

Figure 12: Semileptonic D decay diagrams.

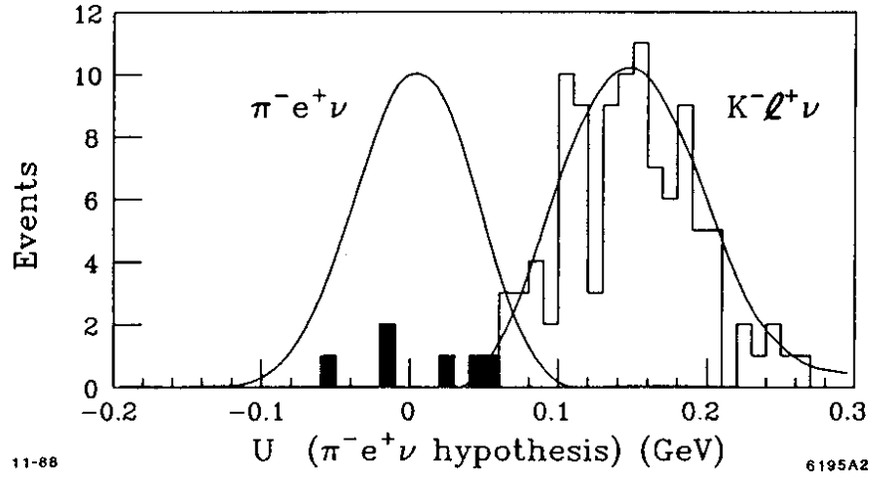

Figure 13: Measurement of $D^0 \to \pi^- e^+ \nu_e$ (shaded events) in Mark III. The distribution of $Ke\nu$ events, after deliberately misidentifying the K as a π, (unshaded data) indicates a clear kinematic separation of these two decay modes.

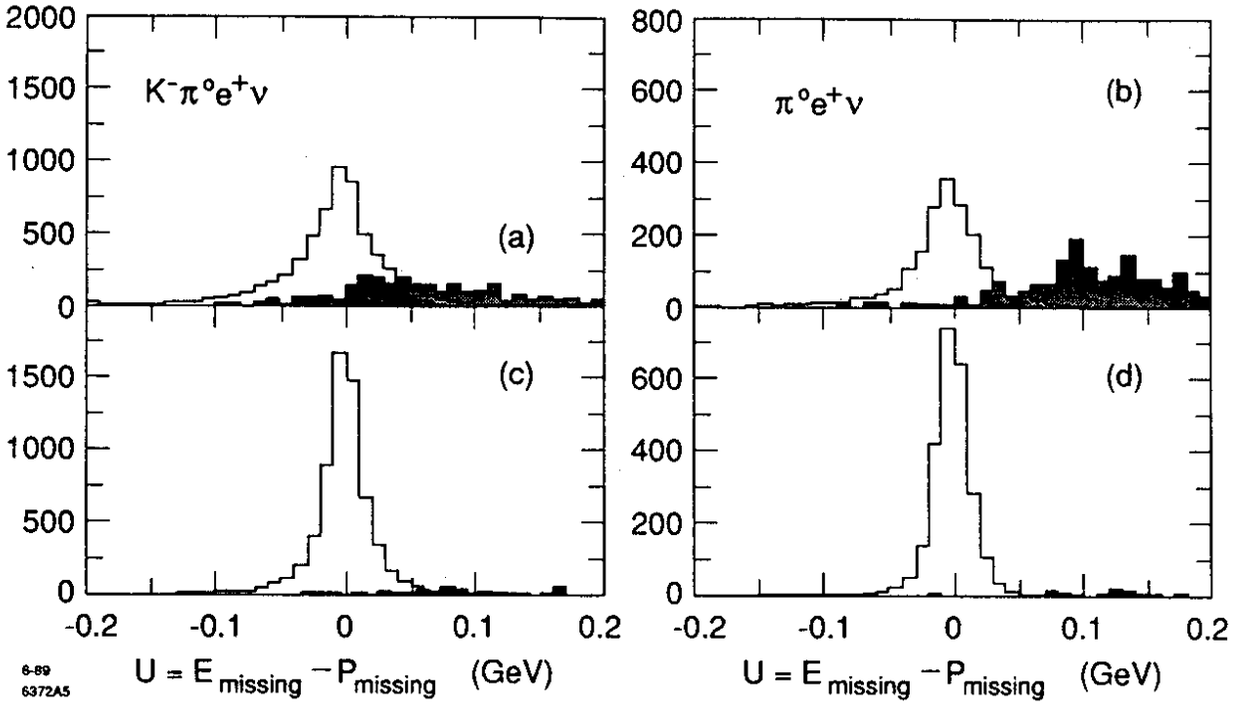

Figure 14: Examples of Cabibbo allowed and suppressed semileptonic decays in the τcF detector, assuming: a) and b) sampling electromagnetic calorimetry; c) and d) crystal electromagnetic calorimetry. The background events are shaded.

KM matrix element	Standard Model [3 generations] (90% CL interval)	Experimental value (90% CL interval)
V_{cs}	0.974 ± 0.001	0.65 – 0.98
V_{cd}	0.220 ± 0.003	0.16 – 0.23

Table 6: Standard Model predictions and experimental values for the Kobayashi-Maskawa (KM) matrix elements V_{cs} and V_{cd}.

clean, the low branching ratio of the Cabibbo-suppressed semileptonic decays ($\leq 1\%$) has precluded their detection until recently, when MkIII observed several $D^0 \to \pi^+ e^- \bar{\nu}_e$ events at SPEAR (Figure 13[17]). There are a large number of semileptonic branching ratios that can be measured at the τcF, which will hopefully provide sufficient redundant information to reduce the theoretical uncertainties on the form factors. The typical statistics will be a few times 10^5 events for Cabibbo-allowed modes, and a few times 10^4 for supressed modes, which will allow both V_{cs} and V_{cd} to be determined to better than 1%, on the assumption of a clearer understanding of the form factors. Each of these modes is expected to have low backgrounds (as seen, for example, in Figure 14[18]), in contrast with similar measurements in fixed-target charm experiments (for example, Figure 15).

Finally we comment that semileptonic $D_s^{\pm}$ decays that proceed through quark annihilation [Figure 12c)] do not suffer from helicity suppression and may have appreciable

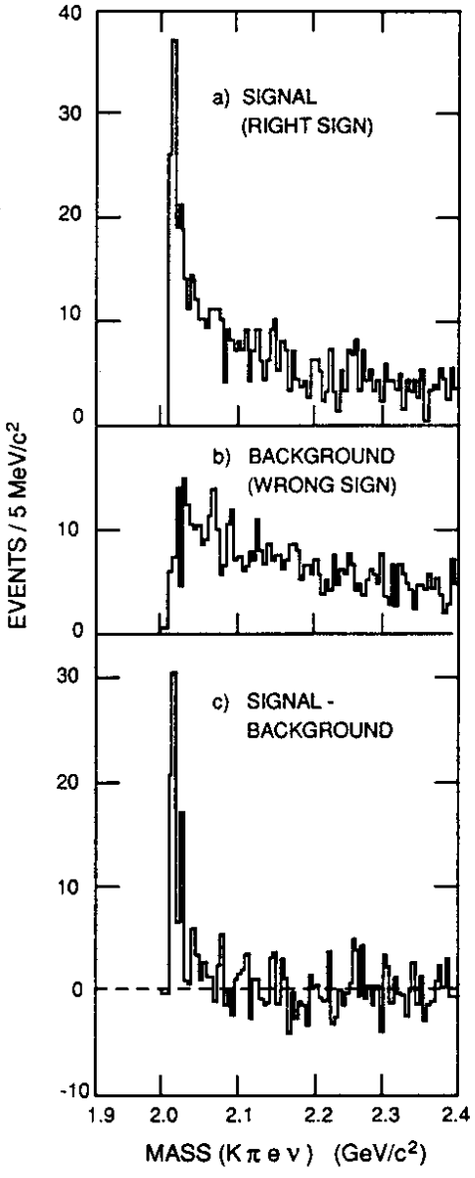

Figure 15: Measurement of the Cabibbo-allowed semileptonic decay $D^0 \to K^- e^+ \nu_e$ in E691 (fixed-target photoproduction). The D^0's are tagged via $D^{*+} \to D^0\ \pi^+$ (right sign; wrong sign for this decay would be $D^0 \pi^-$).

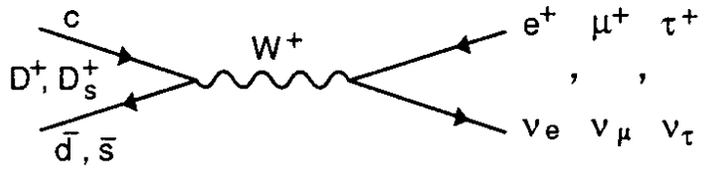

Figure 16: Pure leptonic $D^{\pm}$ or $D_s^{\pm}$ decay diagram.

branching ratios. One of the interests in these processes is the possibility of a clean source of glueballs $D_s^{\pm} \rightarrow glueball\ l^{\pm}\nu_l$.

4.2 Pure leptonic decays

Pure leptonic decays of $D_{(s)}^{\pm}$ mesons (Figure 16) have two distinctive features: they can be rigorously calculated in the Standard Model, and they have not been experimentally observed. The processes of interest are:

$$\Gamma(D^+ \rightarrow \mu^+\nu_\mu) \propto f_D^2 \mid V_{cd} \mid^2,$$

$$\Gamma(D_s^+ \rightarrow \mu^+\nu_\mu) \propto f_{D_s}^2 \mid V_{cs} \mid^2,$$

$$\Gamma(D_s^+ \rightarrow \tau^+\nu_\tau) \propto f_{D_s}^2 \mid V_{cs} \mid^2,$$

where, in the final process, $\tau^+ \rightarrow e^+\nu_e\bar{\nu}_\tau/\mu^+\nu_\mu\bar{\nu}_\tau$. The weak decay constant $f_{D_{(s)}}$ measures the overlap of the c and $d(s)$ quarks in the $D_{(s)}^{\pm}$ meson. The decay constants appear in many second-order weak processes, including mixing and CP violation, and are therefore important quantities to be experimentally determined. Measurement of f_D is needed, for example, to improve the estimate of f_B for calculations of mixing and CP violation in the B system. Furthermore, the relative pure leptonic branching ratios will provide a good measurement of $\mid V_{cs}/V_{cd} \mid$, since the uncertainty in f_{D_s}/f_D should be small. These decays are measured cleanly in the τcF (Figure 17), with expected rates shown in Figure 18[18].

These measurements are also sensitive to new physics that does not have the usual helicity suppression in pseudoscalar meson decay or that has mass-dependent couplings [since we measure the ratio $\Gamma(D_s \rightarrow \mu\nu)/\Gamma(D_s \rightarrow \tau\nu)$][3]. The absence of $e\nu$ final states will provide a further test.

4.3 $D^o\bar{D}^o$ mixing and CP violation.

Searches for mixing and CP violation in the D system[3,19,20] offer several advantages:

- The branching ratios into interesting states are reasonably large, and so observations can be checked in several different ways.
- Quantum statistics results in different correlations for $D^0\bar{D}^0$ decays depending on the whether the process is $\psi''(3.77) \rightarrow D^0\bar{D}^0$; $D^0\bar{D}^{0*} \rightarrow \gamma D^0\bar{D}^0$; or, $D^0\bar{D}^{0*} \rightarrow \pi^0 D^0\bar{D}^0$. These three channels therefore constitute an analyzer to identify the source of a signal.

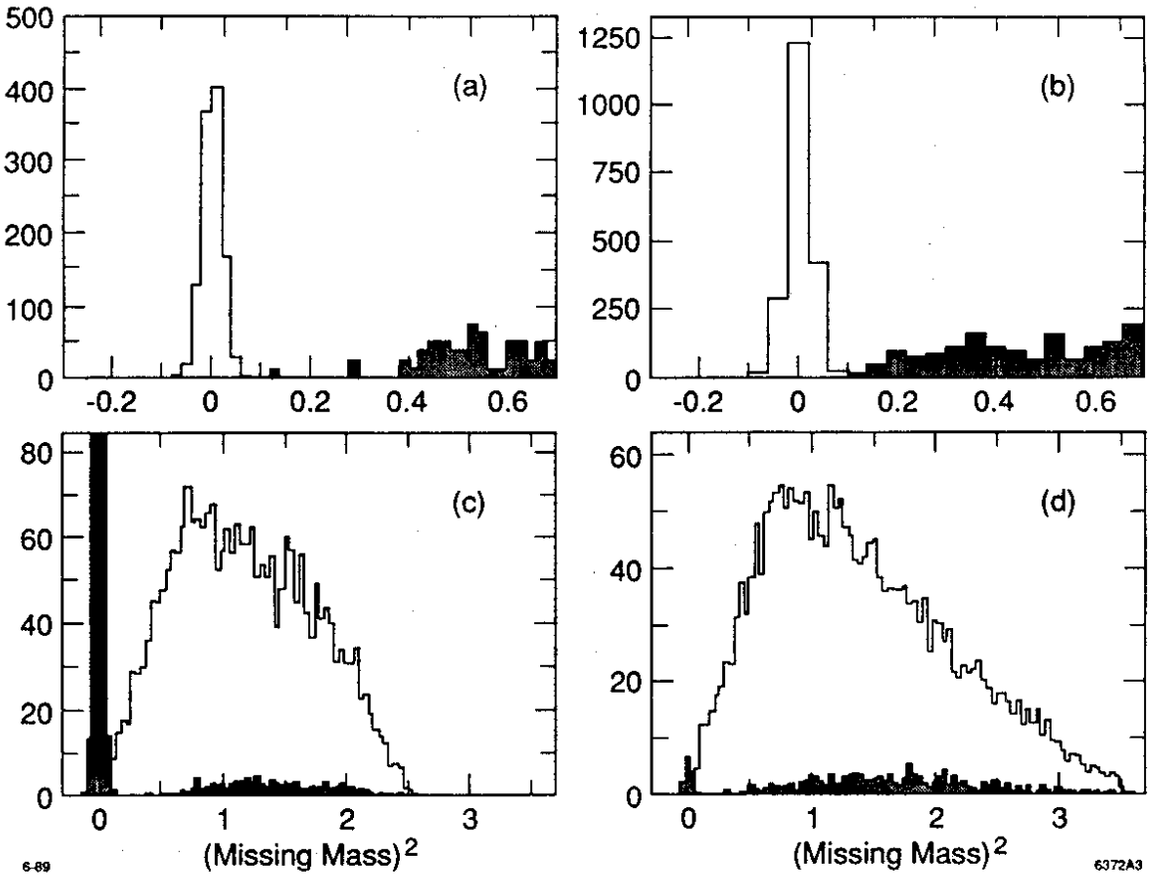

Figure 17: Measurement of pure leptonic D decays in the τcF detector. Missing masses in tagged events are shown for: a)$D^+ \to \mu^+\nu_\mu$; b)$D_s^+ \to \mu^+\nu_\mu$; c)$D_s^+ \to \tau^+\nu_\tau$, $\tau^+ \to e^+\nu_e\bar{\nu}_\tau$; and, d)$D_s^+ \to \tau^+\nu_\tau$, $\tau^+ \to \mu^+\nu_\mu\bar{\nu}_\tau$. The background events are shaded.

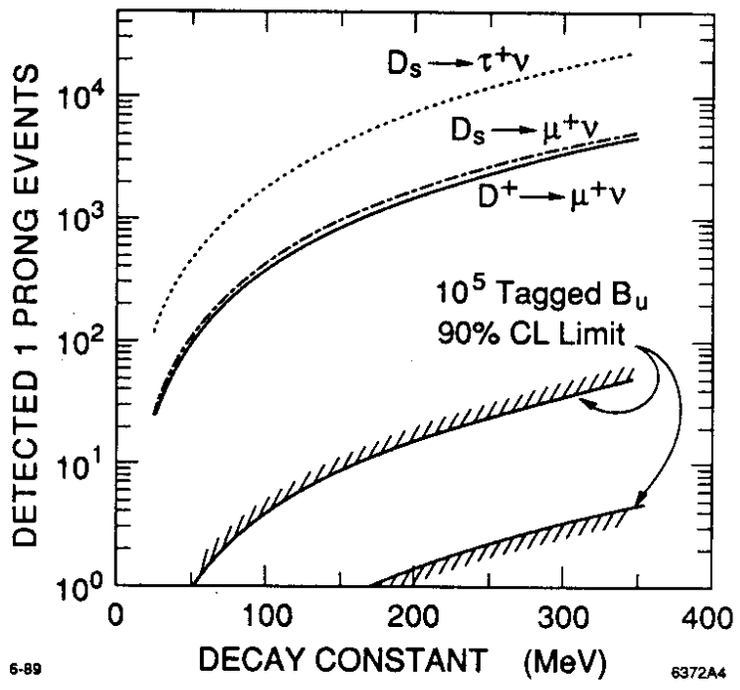

Figure 18: Event samples of pure leptonic D decays vs. the decay constant f_D. After including the τ leptonic branching ratio, all three decays will have similar statistics. Also shown is the sample of pure leptonic $B \rightarrow \tau\nu_\tau$ decays vs. f_B, expected at a B Factory assuming 10^5 tagged B_u (where the indicated limits correspond to the present uncertainty in V_{bu}).

The mixing parameter is defined as

$$r_D = \frac{B(D^0 \to \bar{D}^0 \to \bar{f})}{B(D^0 \to f/\bar{f})} = \frac{(\Delta m_D/\Gamma_D)^2 + (\Delta\Gamma_D/2\Gamma)^2}{2}$$

where f is a final state. Mixing may occur in the Standard Model by 'box diagrams' [Figure 19a)], which are expected to be small ($r_D \leq 10^{-6}$) due to GIM cancellations. Long range contributions (Figure 20), which are also second order weak interactions, are expected to be larger, giving $r_D \simeq 10^{-5} - 10^{-4}$. The small $D^o\bar{D}^o$ mixing expected in the Standard Model make this an ideal channel to search for new physics [e.g. Figure 19b)].

The experimental signatures for mixing are either like-sign dilepton events from dual semileptonic decays ($e^{\pm}e^{\pm}X$, $\mu^{\pm}\mu^{\pm}X$, $e^{\pm}\mu^{\pm}X$) or two *identical* hadronic decays, such as $(K^+\pi^-)(K^+\pi^-)$ or $(K^-\pi^+)(K^-\pi^+)$. Although the source of the leptonic signature is unambiguous, the hadronic signature may signal either mixing or doubly-Cabibbo-suppressed decays (DCSD), which are expected with branching ratios $\simeq \tan^4\theta_c = 0.003$. These two contributions can be separated, however, since Bose statistics *forbids* DCSD when the D^0 mesons are in a relative $l = 1$ state (at $\psi''(3.77)$ and for $D^0\bar{D}^{0*} \to \pi^0 D^0\bar{D}^0$) but *allows* DCSD when the D^0 mesons are in a relative $l = 0$ state ($D^0\bar{D}^{0*} \to \gamma D^0\bar{D}^0$). An independent way to isolate DCSD is to measure their magnitude in the decays of $D^{\pm}$, where mixing is of course absent.

The statistics per year at the τcF are expected to be $\simeq 6\ 10^4$ dilepton events and $\simeq 4\ 10^4$ $(K\pi)(K\pi)$ events[20]. This should allow a sensitivity $r_D \simeq 10^{-5}$. At this level, we may expect in the Standard Model to see a mixing signal.

CP violation in the $D\bar{D}$ system could show up either through mixing or in direct final state decays[3,19,20]. In the case of mixing, the signature is:

1) $D^0 \to l^+X$, with $\bar{D}^0 \to$ CP eigenstate (e.g. K^+K^-).

2) $\bar{D}^0 \to l^-X$, with $D^0 \to$ CP eigenstate (e.g. K^+K^-).

CP violation will give a rate difference between 1) and 2), depending on the quantum state of the $D^o\bar{D}^o$ system.This is described by an asymmetry parameter $A = (\Gamma_1 - \Gamma_2)\ /\ (\Gamma_1 + \Gamma_2)$. A CP asymmetry of $2\sqrt{2r_D}A$ is expected in $D^o\bar{D}^o$ decays from the channel $D^0\bar{D}^{0*} \to \gamma D^0\bar{D}^0$[3]. Adding several CP eigenstates, a yearly sample of 10^4 such events is expected at $E_{cm} = 4.14$ GeV. Assuming $r_D \sim 10^{-4}$, the asymmetry parameter A can be measured to $\sim 3\ 10^{-3}$. Calculations[3] show a similar sensitivity can be reached in the case of measurements of direct CP violation, e.g. detection of $\psi''(3.77) \to D^o\bar{D}^o \to f_{D^0}f_{\bar{D}^0}$, where the final states have equal CP parity, e.g. f=K^+K^-. A single event of this type establishes CP violation, since the initial state is CP even whereas the final state (p wave) is CP odd.

4.4 Rare D decays

Flavour changing neutral current decays can occur at a low rate by second order weak interactions [Figure 21b)-c)], whereas lepton flavour violating decays are completely forbidden (for massless ν's). Examples of the former are $D \to e^+e^-$, $\mu^+\mu^-$, he^+e^-, $h\mu^+\mu^-$, and $h\nu\bar{\nu}$, and of the latter, $D \to e^+\mu^-$, and $he^+\mu^-$. Decays that include hadrons (h) are a

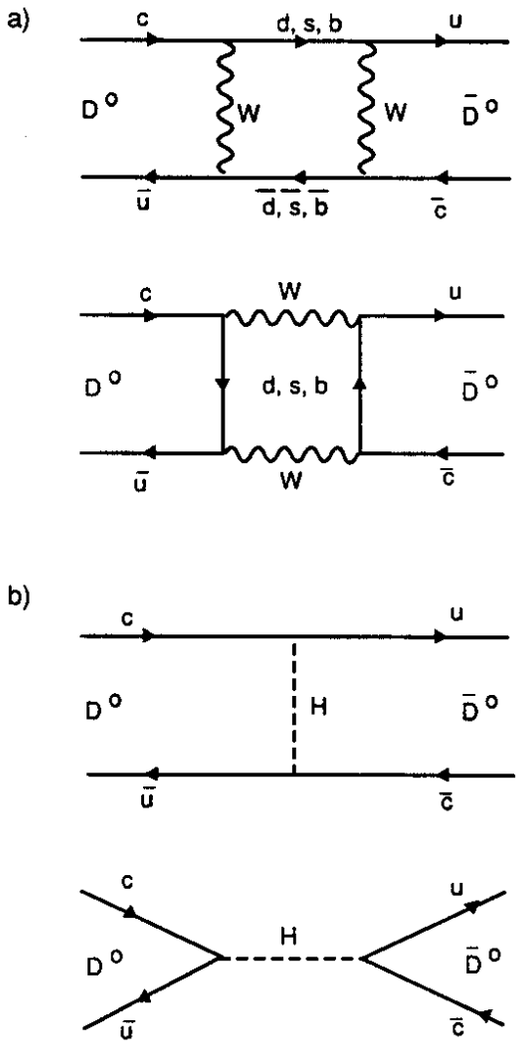

Figure 19: $D^o\bar{D}^o$ mixing by: a) Standard Model 'box' diagrams; and b) new scalar interactions.

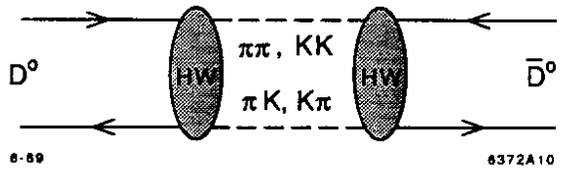

Figure 20: $D^o\bar{D}^o$ mixing diagram by long-range interactions.

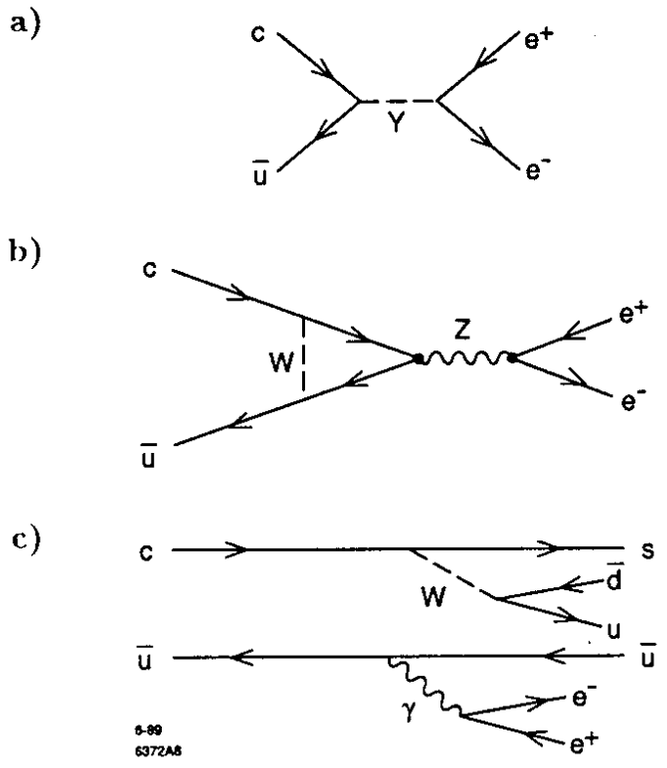

Figure 21: Flavour changing neutral currents by: a) new scalars or vectors; and b) and c) higher-order Standard Model processes.

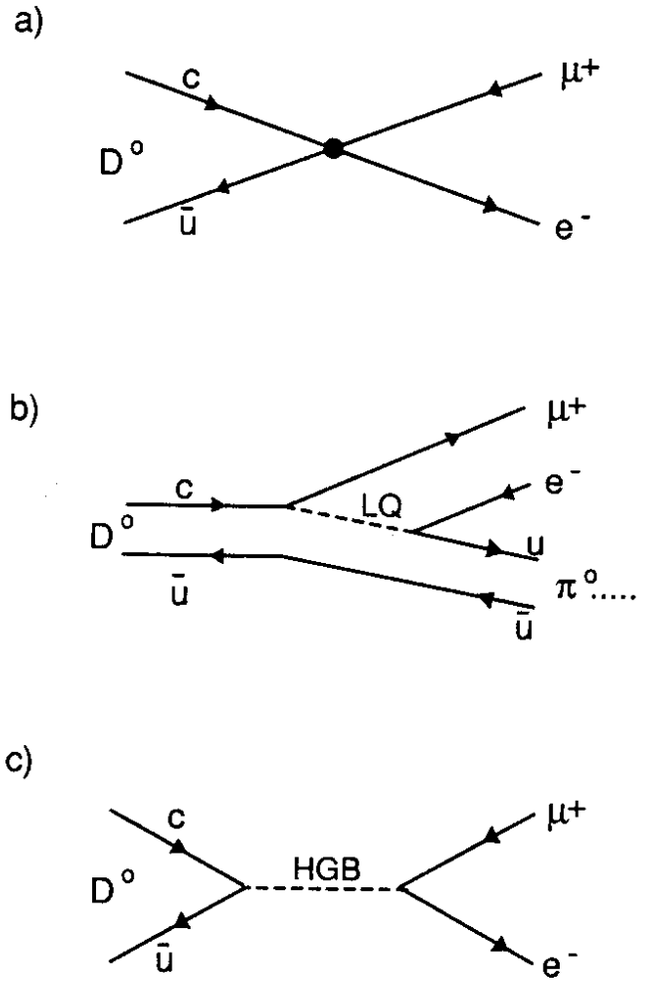

Figure 22: Lepton flavour violating D decay diagrams.

factor 10-100 higher in rate since they do not have any helicity suppression. These decays are sensitive to a broad class of new physics (Figure 22): contact interactions, leptoquarks, horizontal gauge bosons, lepton/quark substructure, Higgs, technicolour, etc. At the τcF these rare decays will have very low backgrounds[18] – generally 1-10 events – and so sensitivities will be at the level of 10^{-7}. This will allow the τcF either to place stringent limits (TeV masses) on such particles, or else provide an observation which will be an unambiguous sign of new physics. In fact, at this experimental sensitivity, several neutral current decays may be observable the Standard Model[19,21]. Finally, we comment that searches for rare decays in the charm sector are complementary to those of K and B mesons since the couplings of the new particles may be flavour dependent, in which case decays of K/B (down-type quarks) will be different from D (up-type quark).

5 J/ψ and ψ' physics

The charmonium states $J/\psi, \psi'$, and η_c provide an exceptionally rich system for clean QCD studies at low Q^2. The areas of interest are as follows[3,22]:

- *Gluons and gluonic particles.* The processes to study are $J/\psi \to gg\gamma$, $J/\psi \to ggg$, and $\eta_c \to gg$.
- *The $c\bar{c}$ wave function and mass spectrum.* Examples are the rates for $J/\psi \to 3\gamma$ (expected br $\sim 10^{-5}$) and $\eta_c \to 2\gamma$ (expected br $\sim 10^{-3}$) for these processes, which are not well known at present, are directly predicted by QCD. An example in the τcF is shown in Fig. 23.
- *Issues in hadronization*, where we look at the details of the hadronic states produced from 2- and 3-gluon intermediate states.

There are several advantages to J/ψ decays for these light quark and glueball spectroscopy studies:

- The initial and final states have well-defined quantum numbers: $J^{PC} = 1^{--}$ and $I^G = 0^-$. The J/ψ is an SU(3) singlet, with no hidden light quarks.
- $J/\psi \to \gamma gg \to \gamma X$ involves a pure two-gluon intermediate state, with a mass $m_{gg} \leq$ 3.1 GeV/c^2, i.e. in the expected mass region of the gluonic spectrum.
- The nature of the state X can be tested experimentally by comparing $J/\psi \to \gamma X, \omega X$ and ϕX. If X is gluonic, then the decays ωX and ϕX will be suppressed; in contrast, ωX is enhanced if X has u/d quark content, and ϕX is enhanced if X has s quark content.
- J/ψ decays have extremely high statistics and almost no background. Current experiments have 10^7 decays, whereas the statistics of the parent sample at the τcF will be 10^{10} per year.

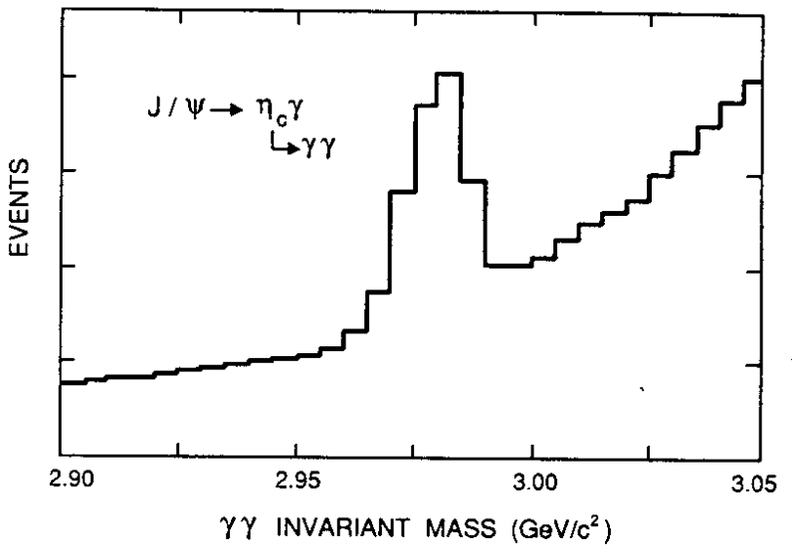

Figure 23: 2γ mass spectrum in the τcF detector from $J/\psi(3.10) \rightarrow \eta_c\gamma$, $\eta_c \rightarrow \gamma\gamma$, including background processes.

With present data samples there are several possible signs of new states, based on signals of a few 10's of events, indicating there is a great deal still to be learnt from J/ψ decays. With the factor 1000 increase in statistics at the τcF it will be possible to carry out a detailed partial wave study of these and other states, which should provide a definitive study of the gluonic spectrum.

There are many further physics possibilities with J/ψ decays. Some examples are:

- *Clean light meson factory.* For example, 10^7 $\Lambda\bar{\Lambda}$ events per year are produced from J/ψ decays.
- *Weak decay studies*, e.g. $J/\psi \rightarrow D_s e\nu_e$ (br $\sim 10^{-8}$).
- *Tagged J/ψ decays*, via $\psi' \rightarrow \pi^+\pi^- J/\psi$. One interesting decay is $J/\psi \rightarrow \nu\bar{\nu}$ (br $\sim 10^{-8}$).
- *Axion search*, via $J/\psi \rightarrow \gamma$ *axion*. The current experimental limit (Crystal Barrel) for this branching ratio is $< 1.4\ 10^{-5}$ (90% CL).

6 Machine

The τ-charm Factory will explore the second generation quark family and the third generation lepton family with unprecedented sensitivity. The success of this endeavour will depend on the combination of **two** features of the experimental apparatus:

τcF physics sensitivity $\propto$ machine luminosity x detector performance

The high luminosity of the τcF, combined with its unique operating points, will generate a large increase in the available statistics of τ and charm data samples, under conditions of low backgrounds and low systematic biases. As examples, the present total luminosity is 2 pb^{-1} for $\tau^{\pm}$ studies below charm threshold, and 10 pb^{-1} for charm studies at $\psi''(3.77)$. These figures may be compared with the design luminosity of 10^4 pb^{-1} per year at the τcF.

Furthermore, a substantial improvement can be made in detector performance compared with previous experiments. In particular, we note that no previous detector in the τ-charm region has combined the advantages of the classical solenoidal magnetic detector – good momentum resolution and identification of charged particles – with the advantages of the crystal calorimeter detector – excellent energy resolution for γ, e, and π^0, and good low energy γ detection efficiency. This style of detector – which has been pioneered by the work of L3 and CLEO II – would have a profound effect on the scope of physics accessible at the τcF, due to a sharp increase in the reconstruction efficiency and resolution of final states that include neutrals and due to improved e identification.

The original τcF machine design was made by Jowett[4,5,23]. This was evaluated and further developed at the SLAC *Tau Charm Workshop*, at which time several new ideas were introduced – most notably a 'crab-crossing' scheme[25] – that may lead to improved performance. The detailed results of these studies, as well as a machine summary[24], are contained in ref.[1]. In this and the following section, we will outline the main features of the machine and detector designs that emerged from this Workshop.

6.1 Design specifications

The basic design specifications of the τcF machine are as follows:

- An e^+e^- collider operating in the range $3.0 \leq E_{cm} \leq 4.25$ GeV, with equal e^+ and e^- beam energies.
- A peak luminosity $L \geq 10^{33}\,\mathrm{cm}^{-2}\mathrm{s}^{-1}$ to occur at $E_{cm} = 4.0$ GeV. At lower energies the luminosity is

  $$L = (E_{cm}/4.0)^2\, 10^{33}\mathrm{cm}^{-2}\ \mathrm{s}^{-1}$$

  which implies 0.6 $10^{33}\,\mathrm{cm}^{-2}\mathrm{s}^{-1}$ at $J/\psi(3.10)$ and 0.8 $10^{33}\,\mathrm{cm}^{-2}\mathrm{s}^{-1}$ at $\tau^+\tau^-$ threshold. At higher energies the luminosity is

  $$L = (4.0/E_{cm})^n\, 10^{33}\mathrm{cm}^{-2}\ \mathrm{s}^{-1}$$

  where $3 \lesssim n \lesssim 4$, implying 0.8 $10^{33}\,\mathrm{cm}^{-2}\mathrm{s}^{-1}$ at $E_{cm} = 4.25$ GeV.

- A dedicated e^+ and e^- injector that operates at collision energy. This allows frequent 'topping-off' of the stored beam (every 30-60 minutes) and thereby maintains an average luminosity above 80% of the peak value. A dedicated injector will also facilitate continuous operation of the τ-charm Factory ($\gtrsim$ 10 months per year).

The original concept of the τ-charm Factory was an integrated detector and machine with a single interaction point[4,26]. This approach was largely supported at the *Tau Charm Workshop* since it will result in the highest possible luminosity per interaction point, while simplifying the machine design and reducing the cost. Where resources are limited, it is better to deliver the highest luminosity to a single high-performance detector rather than to compromise the performance of each by adding a second interaction region and a second detector. For a second detector, at this stage it is hard to identify either a design that is complementary to the first, or where special emphasis should be placed. At present it is felt that the best approach is to construct a single interaction region with a 'push-pull' capability. In this way a second, special purpose, detector can be brought in to alternate with the general purpose detector, after an appropriate physics goal has been identified.

6.2 Design criteria of a high luminosity storage ring

We will now consider the general design criteria to produce high luminosity in a storage ring collider. The symbols used here are defined in Table 7.

The event interaction rate between two counter-rotating trains of e^+ and e^- bunches is:

$$(N_b\,\sigma_{int}/A)\,(N_b)\,(f_b) = (N_b\,\sigma_{int}/A)\,(N_b)\,(c/S_b),$$

where A is the beam transverse area and σ_{int} is the interaction cross section. The luminosity is therefore:

$$L = (c\,N_b^2)\,/\,(S_b\,A) = (c\,N_b^2)\,/\,(S_b\,4\pi\sigma_x^*\sigma_y^*).$$

In practice, there are limits to each of the adjustable quantities in this expression, and a more useful expression for the luminosity can be derived (see, for example, ref.[4]) that involves the vertical beam-beam tune shift

$$\xi_y = \frac{N_b r_e \beta_y^*}{2\pi(E_0/m_e c^2)(\sigma_x^* + \sigma_y^*)\sigma_y^*}$$

(The corresponding horizontal beam-beam tune shift is defined similarly, with the interchange of x and y.) This tune shift, which results from non-linear resonances driven by the beam-beam force, is found to have a practical upper limit of 0.03-0.05 in e^+e^- storage ring colliders. A measure[27] of the scale of this effect is that, at the tune-shift limit, the disruption angle of the colliding beams is approximately (within a factor of 2) equal to the 'natural' angular spread ($\sqrt{\epsilon/\beta^*}$) of the stored beams at the interaction point. The maximum luminosity is achieved when $\xi_x = \xi_y$, and this condition is reached for 'optimum coupling':

$$\kappa = \sqrt{\frac{\epsilon_{yc}}{\epsilon_{xc}}} = \sqrt{\frac{\beta_y^*}{\beta_x^*}}.$$

E_0	beam energy
R	average radius (circumference/2π)
$f_0 = c/2\pi R$	revolution frequency
e, m_e	electron charge and mass
$r_e = e^2/m_e c^2$	classical radius of the electron
k_b	number of bunches
$S_b = 2\pi R/k_b$	bunch separation
$f_b = c/S_b$	bunch crossing frequency
N_b	number of particles per bunch
$I_b = N_b e f_0$	current per bunch
$I = k_b I_b$	total beam current
κ	betatron coupling parameter
ϵ_x	total horizontal emittance (no coupling)
$\epsilon_{xc}, \epsilon_{yc}$	coupled radial, vertical horizontal emittance
σ_x^*, σ_y^*	r.m.s. radial, vertical beam sizes at interaction point
β_x, β_y	radial, vertical β-function
β_x^*, β_y^*	β-functions at interaction point
σ_ϵ	r.m.s. fractional energy spread
σ_z	r.m.s. bunch length
$f_{\mathrm{RF}} = c/\lambda_{\mathrm{RF}}$	RF frequency
V_{RF}	total peak RF voltage
ξ_x, ξ_y	radial, vertical beam-beam tune-shift
L	luminosity

Table 7: List of machine symbols and notations

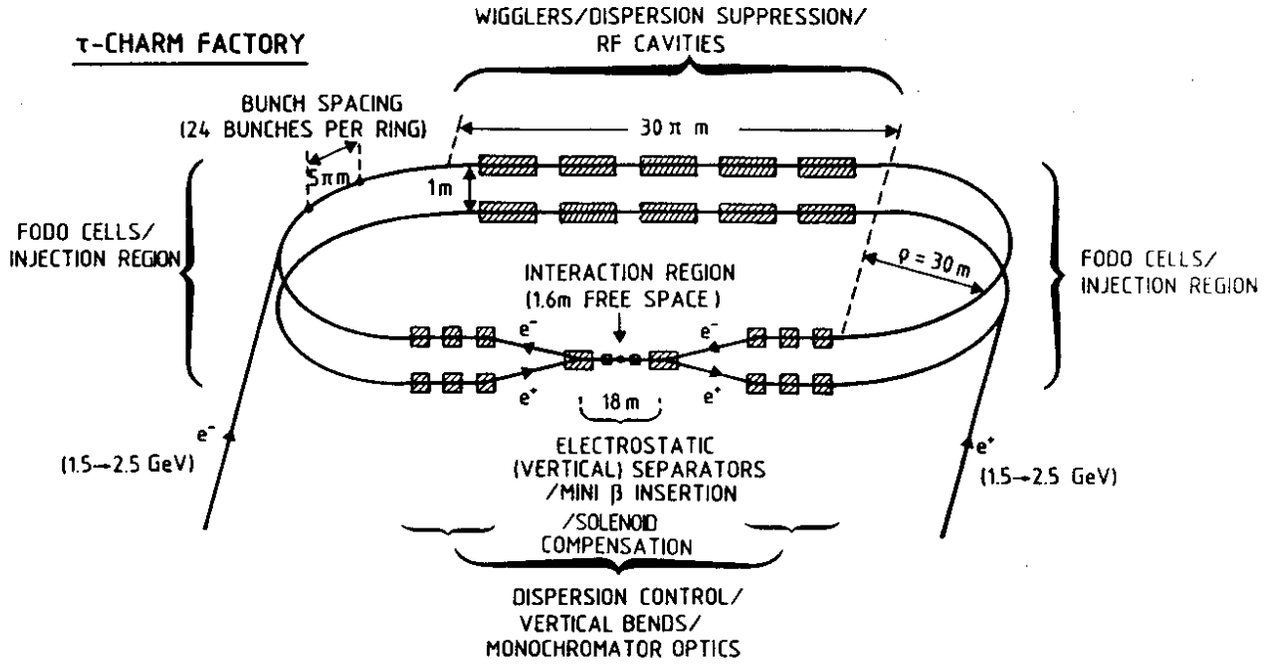

Figure 24: Schematic design of the τ-charm Factory storage ring.

Numerically, after the appropriate substitutions[4], the luminosity under these conditions is:

$$[L/\mathrm{cm}^{-2}\mathrm{sec}^{-1}] = 4.54 \times 10^{40} \frac{[1+\kappa^2][\epsilon_x/\mathrm{m}][\xi_y^2][E_0/\mathrm{GeV}]^2}{[S_b/\mathrm{m}][\beta_y^*/\mathrm{m}]}. \quad (1)$$

The design criteria for a high-luminosity storage ring can readily be seen from equation (1) as follows:

- *Minimum bunch spacing* S_b. Two rings with a single interaction point permit operation with many bunches. A vertical separation scheme on each side of the interaction point avoids parasitic crossings.
- *Maximum beam-beam tune shift* ξ_y. This is achieved by having a zero-degree crossing angle, a large dynamic aperture, good magnet alignment and flexible orbit control.
- *Maximum horizontal emittance* ϵ_x. This is satisfied by a large machine aperture, two rings (i.e. no pretzel scheme), and wigglers, which maintain a large emittance at lower energies.
- *Minimum* β_y^**, i.e. maximum vertical focussing at the interaction point.* This necessitates close-in final-focus quadrupoles, and also a short bunch length which, in turn, requires a low-impedance vacuum chamber.

6.3 Optics

A schematic design of the τcF machine is shown in Figure 24 and a summary of the main parameters is given in Table 8. The original design used doublet focussing to achieve

Energy	E	2.5	GeV
Circumference	C	376.99	m
Revolution frequency	f_0	1.2575	μsec
Bending radius	ρ	12	m
β-function at IP	β_x^*	0.2	m
	β_y^*	0.01	m
Betatron coupling	κ^2	0.045	
Betatron tunes	Q_x	$\simeq 10.8$	
	Q_y	$\simeq 9.4$	
Momentum compaction	α	0.0189	
Natural emittance	ϵ_x	281	nm
Energy spread	σ_ϵ	5.66×10^{-4}	
Energy loss per turn	U_0	0.288	MeV
Damping times	τ_x	35	msec
	τ_y	22	msec
	τ_ϵ	9	msec
RF frequency	$f_{\rm RF}$	1.489	GHz
RF voltage	$V_{\rm RF}$	5	MV
Radiation power	$P_{\rm rad}$	0.309	MW (2 beams)
Synchrotron tune (RF2)	Q_s	0.106	
Stable phase angle	ϕ_s	3.3°	
Number of bunches	k_b	24	
Bunch separation	S_b	15.71	m
Bunch spacing	τ_b	52.4	nsec
Bunch crossing frequency	f_b	19.1	MHz
r.m.s. bunch length	σ_z	6.1	mm
Total beam current	I	537	mA
Particles per bunch	N_b	1.75×10^{11}	
Beam sizes at IP	σ_x^*	232	μm
	σ_y^*	$\simeq 10$	μm
Beam-beam parameter	ξ_y	0.04	
Luminosity	L	1.2×10^{33}	$\rm cm^{-2}sec^{-1}$

Table 8: τcF machine parameter list at top energy in the Jowett design[23]. This list refers to the original energy that corresponds to the peak luminosity, 2.5 GeV; in the present design the top energy is reduced to 2.0 GeV.

$\beta_y^* = 1\,\mathrm{cm}$, with the superconducting quadrupole magnets ($\mu\beta$ quads) protruding into the detector. The detector constraints fix the inner face of the first quadrupole at 0.8 m from the interaction point, and fix the outer radius of the $\mu\beta$ quads at 20 cm. We envisage[28] a set of iron-free superconducting quadrupoles whose coils can be separately rotated inside their common cryostat to compensate the betatron coupling induced by the detector solenoid. For these optics, superconducting $\mu\beta$ quads are required with a gradient $30\,\mathrm{T\,m^{-1}}$ which gives a maximum field in the winding $B_{Q1} \simeq 2.5\,\mathrm{T}$. This should be achievable without a cold bore.

In the initial optics, the ratio $\beta_y^*/\beta_x^* = 1\mathrm{cm}/80\mathrm{cm}$ was too small – it assumed an unreasonably weak coupling between the horizontal and vertical betatron oscillations – and so an additional quadrupole has been introduced[23] to give $\beta_y^* = 1\,\mathrm{cm}$, $\beta_x^* = 20\,\mathrm{cm}$. The resulting optics and beam sizes in the experimental insertion are shown in Figures 25 and 26, respectively. Figure 26 shows that the proposed vacuum chamber of 50 mm half-aperture satisfies the beam-stay-clear requirement of $10\sigma_{x,y} + 2\mathrm{mm}$. The additional quadrupole magnet is introduced before the beam separator, extending the length of the $\mu\beta$ quad assembly to $\simeq 0.9\mathrm{m}$ and reducing the separator length to 4 m.

The lower limit on S_b is set by the accumulated length of the micro-β insertion and the separation scheme which follows it. Electrostatic plates are used to provide the initial weak vertical separation of the beams before magnetic elements (quadrupoles and vertical-bending magnets) direct the beams to or from their separate rings. The total length of a (half) insertion is 7.6 m including a conservative allowance for the length and strength ($E_y \leq 2\,\mathrm{MV\,m^{-1}}$) of the electrostatic separator plates. At the Workshop, in fact, it was felt that this separation scheme could be realistically pushed to allow a reduction of S_b by a factor of 2, thereby increasing the number of bunches to 48 and raising the luminosity by a factor of 2.

The remainder of the two storage rings contains the standard optical sections: FODO arc cells, four dispersion suppressors for the straight sections, injection insertions etc. The long utility straight sections have several matching cells (Q-adjustment, control of optical functions etc.) as well as space for the RF system, wigglers etc. Robinson wigglers are used to keep the emittance constant ($L \propto E^2$) and also to reduce the energy spread (maintain short bunches). A small bending radius $\rho = 12$ m provides rapid damping between beam-beam collisions.

During the *Tau Charm Workshop* several new ideas emerged for improving the performance of the τcF machine. An alternative scheme for the beam separation was suggested by Kroll[29], involving crossed electric and magnetic fields, that has the merit of directing away from the interaction region the synchrotron radiation from vertical bending. Siemann[30] presented simulation results suggesting that a higher beam-beam limit can be reached with round beams instead of the more-usual flat ones.

Voss[25] proposed that the best way to increase the luminosity may be to push the bunch spacing S_b to its smallest possible value [equation (1)]. This can be done in a crab-crossing beam geometry, in which the beams have a finite horizontal crossing angle (2α). In order to prevent the excitation of synchro-betatron resonances, the bunches are rotated in RF 'crab' cavities, by an angle α around their centres, just before colliding and then restored by a counter rotation after colliding. In this way the collisions occur head-on with

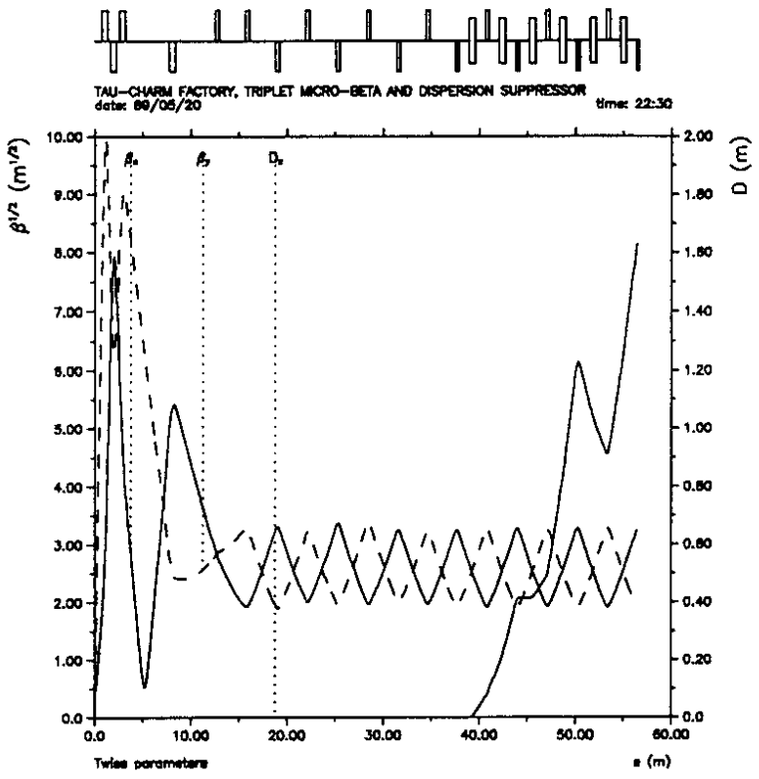

Figure 25: Optics of the experimental insertion and dispersion suppressor (triplet focussing).

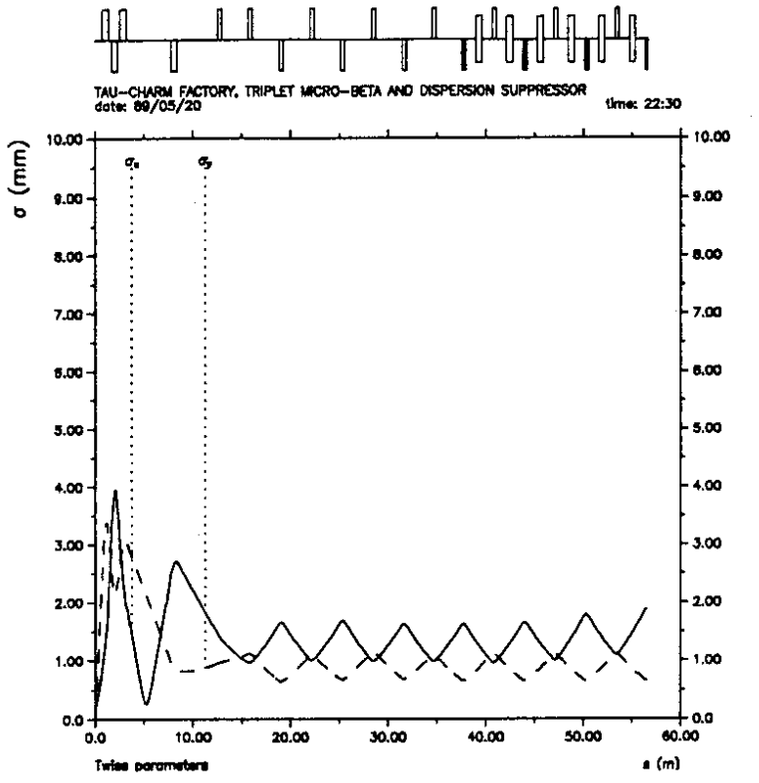

Figure 26: Beam sizes (vertical assumes full coupling) for the triplet $\mu\beta$ optics.

Energy	E	2.2	GeV
Circumference	C	377.4	m
β-function at IP	β_x^*	1.0	m
	β_y^*	0.03	m
Betatron coupling	κ^2	0.03	
Momentum compaction	α	0.026	
Natural emittance	ϵ_x	250	nm
Energy spread	σ_ϵ	5.4×10^{-4}	
Energy loss per turn	U_0	0.174	MeV
RF frequency	$f_{\rm RF}$	353	MHz
RF voltage	$V_{\rm RF}$	2	MV
Radiation power	$P_{\rm rad}$	2.2	MW (2 beams)
Number of bunches	k_b	444	
Bunch separation	S_b	0.85	m
Bunch spacing	τ_b	2.83	nsec
Bunch crossing frequency	f_b	353	MHz
r.m.s. bunch length	σ_z	2.1	cm
Total beam current	I	6.5	A
Particles per bunch	N_b	1.15×10^{11}	
Beam sizes at IP	σ_x^*	500	μm
	σ_y^*	$\simeq 15$	μm
Horizontal crossing half-angle	α	6	mr
Max. crab cavity voltage	V_{cr}	0.71	MV
Beam-beam parameter	ξ_y	0.04	
Luminosity	L	4.6×10^{33}	$\rm cm^{-2}sec^{-1}$

Table 9: Parameters of a τ-charm Factory with horizontal crab-crossing by Voss et al.[25]. In this scheme *all* the RF buckets are filled with beam.

a simultaneous (inconsequential) transverse motion in the laboratory frame. The design parameters of this machine are summarized in Table 9. The advantages of this scheme are an increased luminosity while relaxing the requirements on β_y^*, the bunch length, and the vacuum chamber impedance; and removing the needs for electrostatic beam separators and for high-frequency superconducting RF cavities. The new challenge is clearly a beam current that is an order of magnitude larger than any previous e^+e^- storage ring. The results of experimental tests of this new idea – perhaps at PEP or PETRA – are eagerly awaited.

6.4 Beam currrent limitations and RF

The stored beam current will ultimately be limited by single- or multi-bunch collective effects, which therefore received considerable attention at the Workshop.

The operation of the $\mu\beta$ optics requires short bunch lengths $\sigma_z \simeq 1$ mm to be maintained and this, in turn, implies a low longitudinal impedance $Z/n \simeq 0.2 - 0.4\Omega$. An impedance budget for the vacuum chamber and a *superconducting* RF system carried out at the Workshop showed that these low values could be achieved with careful design. A high frequency (1.5 GHz) superconducting system, similar to the CEBAF design, can provide a short bunch length with low impedance since it comprises only a few cells.

In a machine with so many bunches, coupled-bunch instabilities are likely to be important. The conclusion at the *Tau Charm Workshop* was, for a τcF with CEBAF cavities, that the correction of multi-bunch instabilities would probably need both a feedback system *and* new approaches to damping or controlling the modes. An additional instability that was found to require further study is positive ion trapping in the e^- storage ring. Ion trapping gives rise to nonlinear resonance excitation, reduced beam lifetime and increased backgrounds.

The high beam currents will lead to heating of the vacuum chamber components by synchrotron radiation and parasitic mode losses, and so the vacuum chamber must be designed with suitable cooling.

6.5 Injector

Three injection schemes (Figure 27) were considered at the Workshop:

a) A simple linac with a 1 μs pulse.

b) A linac, with a positron accumulator and damping ring, followed by a SLEDed linac.

c) A linac, with a positron accumulator and damping ring, followed by a booster synchrotron.

Each injector is capable of filling the τcF storage rings in less than 1 minute. The estimated (US) costs are : a) \$20M, b) \$25M, and c) \$27M.

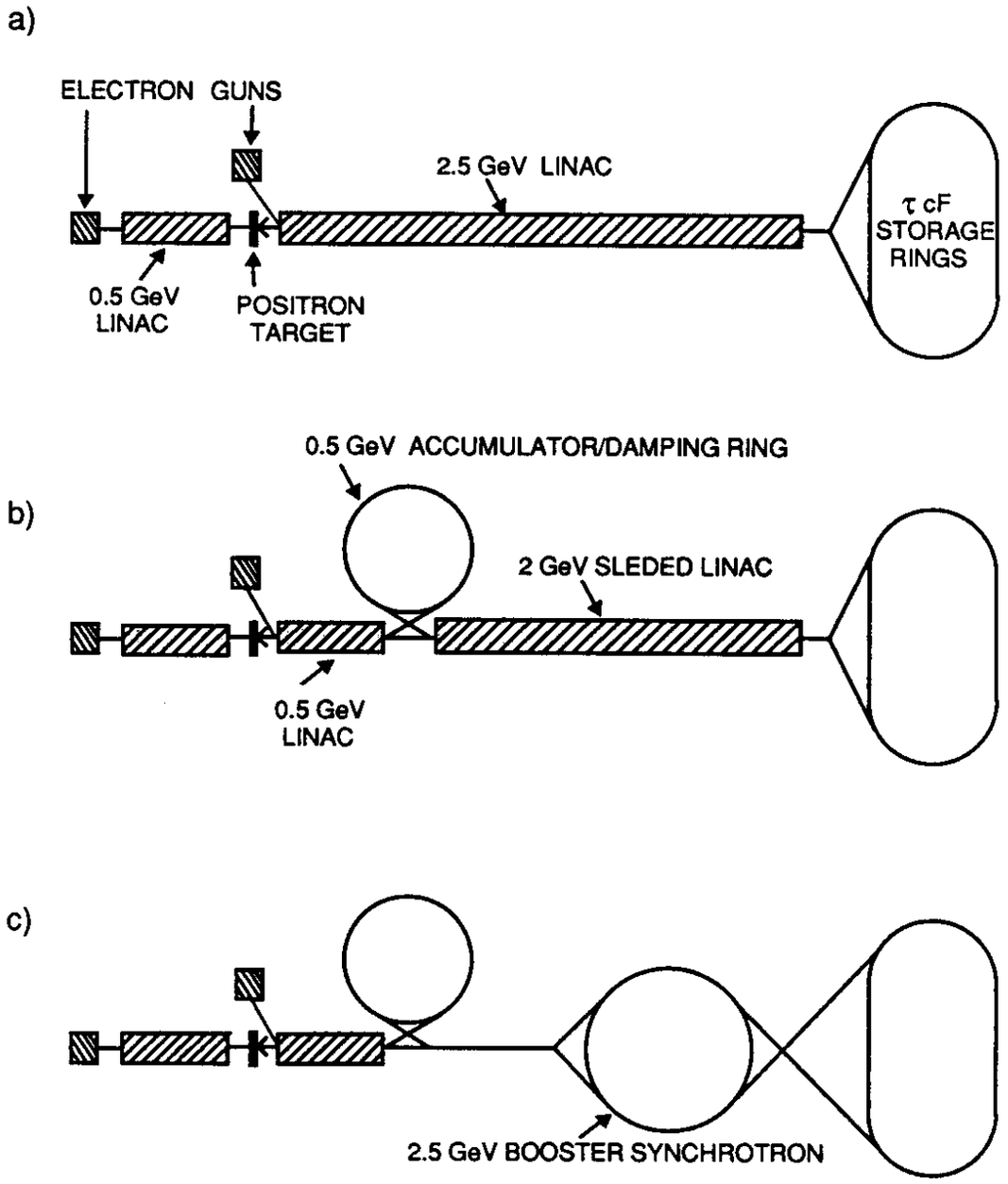

Figure 27: Schematic designs (not to scale) of possible injector layouts for the τ-charm Factory. The overall length of the injector complex is 100-150 m. At present, design b) is preferred.

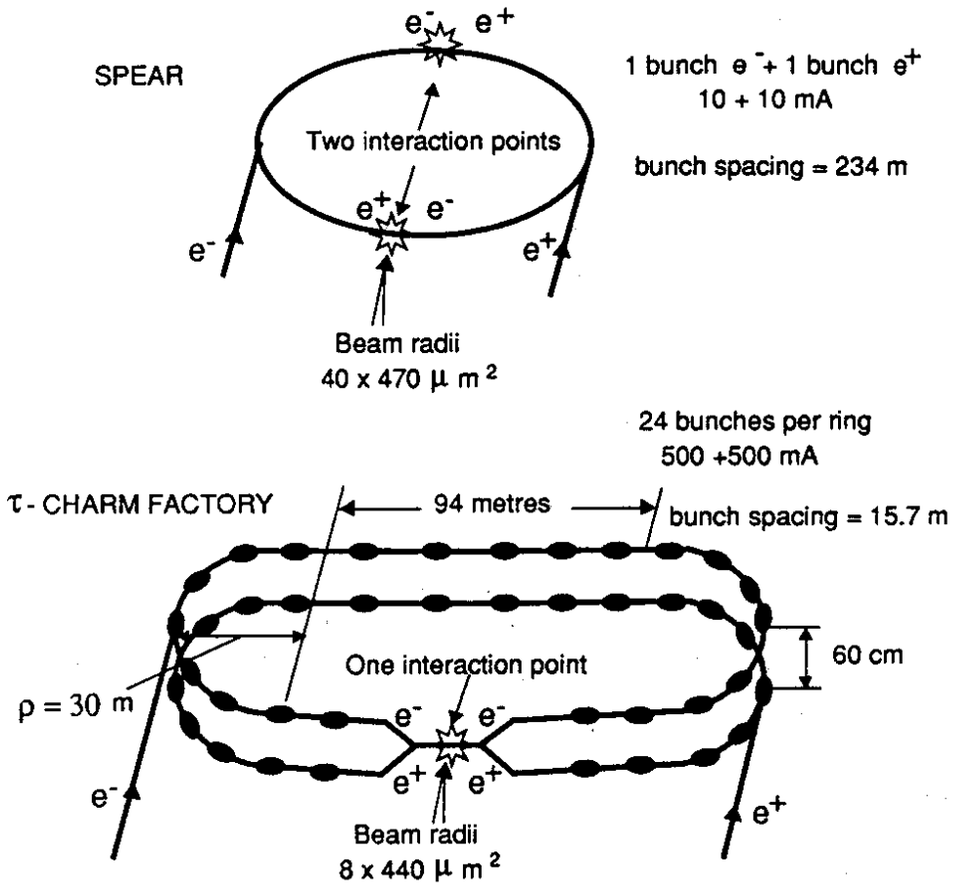

Figure 28: A comparison of the τcF and SPEAR storage rings.

6.6 Controls

In order to maintain the average luminosity close to the peak value, both an efficient injector *and* a highly automated control system will be necessary. Present control systems in general involve a considerable amount of manual adjustment by the operator after injection: orbits, tune, coupling, RF phase, beam lifetime, backgrounds, etc. With injection at the τcF foreseen every 30-60 minutes, this manual optimization would simply be too slow.

6.7 Comparison with SPEAR

It is instructive to compare the parameters of the τcF with SPEAR (Figure 28) in order to see where the increase in luminosity is being achieved. Recalling equation (1), i.e. $L \propto (\epsilon_x \xi_y^2 / S_b \beta_y^*)\, E_0^2$, the improvements are due to:

- *Reduced bunch spacing.* The improvement in S_b is 15.7m : 234m, i.e. a factor 15.
- *Increased beam-beam tune shift.* The improvement expected in ξ_y is $(0.05)^2 : (0.025)^2$, i.e. a factor 4.

- *Increased horizontal emittance* The natural emittance ϵ_x of the τcF is 280 nm, compared with the SPEAR value of 200 nm at $E_0 = 2.0$ GeV. The improvement is a factor 1.4.

- *Reduced* β_y^*. The improvement in β_y^* is 1cm : 10cm, i.e. a factor 10.

These factors combine to give an overall luminosity increase over SPEAR of about 1000. With many bunches, the τcF has a high beam current: 540 mA (compared with a SPEAR current of 10 mA at $E_{cm} = 4$ GeV).

The conclusions from the *Tau Charm Workshop* were that a luminosity $\gtrsim 10^{33}\,\mathrm{cm}^{-2}\mathrm{s}^{-1}$ is realistic for the τ-charm Factory, using present techniques, and that several new ideas exist that may extend the luminosity even higher.

The success of the τ-charm Factory – like any particle factory – will depend on achieving a luminosity close to its design value. Such machines cannot redeem themselves simply by virtue of having opened up a new energy region. It follows that there is no room for compromises and that careful and thorough design and engineering – of both the machine and the detector – will be mandatory throughout the project.

7 Detector

7.1 Design requirements

The primary requirements on the detector design[31] that emerged from the physics studies (Table 10) and discussions at the *Tau Charm Workshop* are as follows:

1. **Precise momentum measurement accuracy**, with particular emphasis on minimizing the effects of multiple Coulomb scattering:

$$[\sigma_p/p]^2 \;=\; [0.4\%p(\mathrm{GeV/c})]^2 + [0.3\%/\beta]^2$$

   The main experiment that requires this high precision for σ_p/p is the measurement of the ν_τ mass to a sensitivity of 1 MeV/c^2.

2. **Crystal electromagnetic calorimeter**, with high resolution of γ energies:

$$[\sigma_E/E]^2 \;=\; [2\%/\sqrt{E\,(GeV)}]^2 + [1\%]^2$$

   and a low threshold energy for γ detection:

$$E_\gamma^{min} \;\simeq\; 10\mathrm{MeV}$$

Experiment	Detector emphasis				
	Charged particles	Photons	πKp i.d.	$e\mu$ i.d.	Hermeticity
$\underline{\tau^{\pm}\text{ physics:}}$					
ν_τ, $\tau^{\pm}$ masses	•	•	•	•	•
$\tau \rightarrow l\nu_l\nu_\tau$ spectra		•		•	•
Precise branching ratios		•	•	•	•
Second class currents		•		•	•
Weak hadronic current	•	•	•	•	•
$\tau^{\pm}$ electric dipole moment		•	•	•	•
Rare decays	•	•	•	•	•
$\underline{D, D_s\text{ physics:}}$					
V_{cs}, V_{cd} (semileptonic decays)		•	•	•	•
f_D (pure leptonic decays)		•		•	•
Hadronic decays (CA, CS, DCS)	•	•	•		
$D^o\bar{D}^o$ mixing, CP violation	•		•	•	•
Rare decays	•			•	•
$\underline{J/\psi(3.10),\ \psi'(3.69)\text{ physics:}}$					
Spectroscopy ($c\bar{c}$, gg, hybrid, uds)	•	•	•		
Rare decays		•	•	•	•

Table 10: Special detector requirements for individual τcF experiments. The presence of '•' signifies that the experiment requires special emphasis on this feature of the detector. In this context,'special emphasis' implies a performance that is substantially better than Mark III.

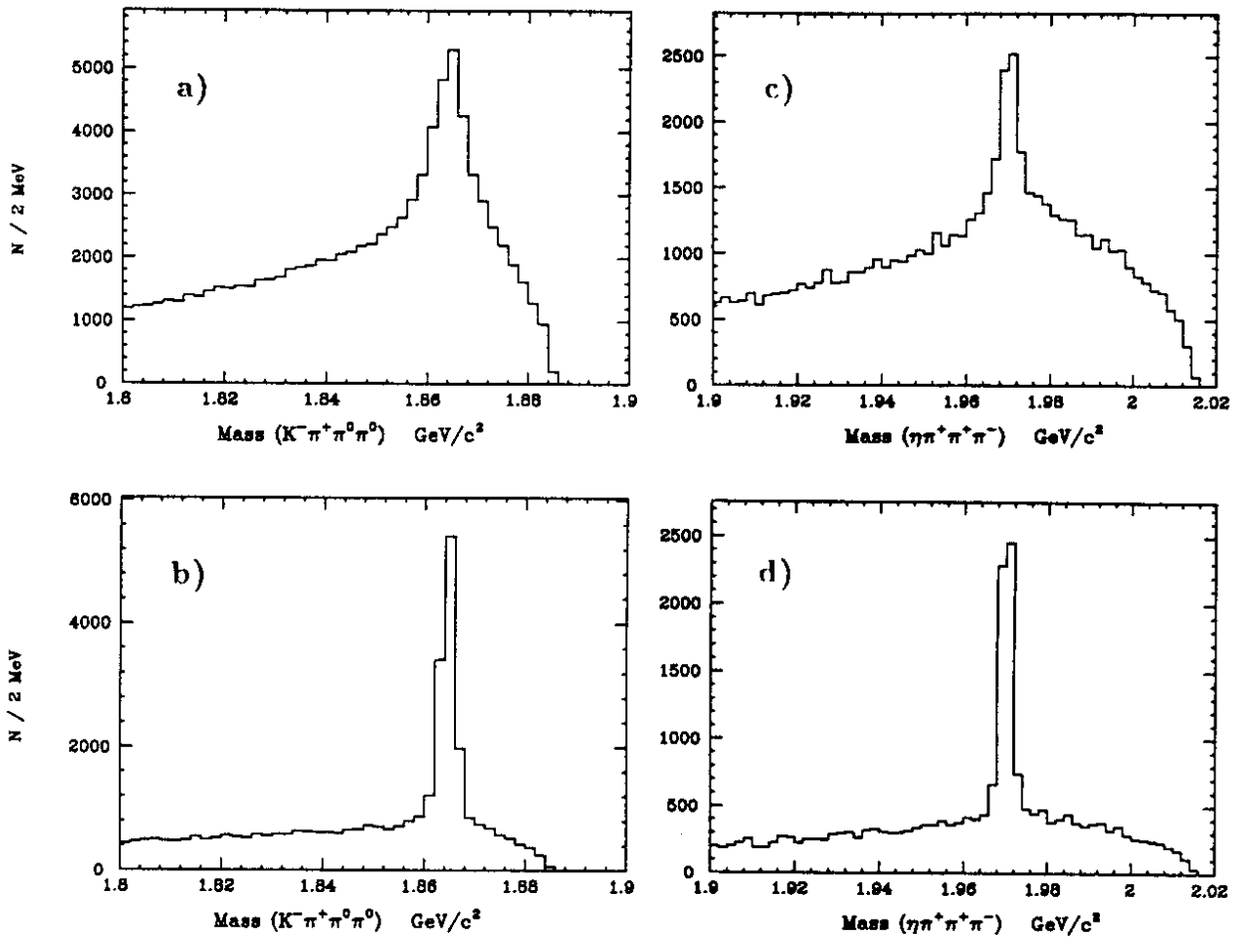

Figure 29: The effect of improved γ energy resolution on tagging D and D_s decays that involve neutral particles[34]. Curves a) and c) correspond to $8\%/\sqrt{E}$ energy resolution, whereas b) and d) correspond to $2\%/\sqrt{E}$. All curves assume the same detection efficiency, which reaches 50% at 50 MeV [pessimistic for the crystal calorimeter curves b) and d)]. Reconstructed masses are shown for: a) and b) $D^0 \to K^-\pi^-\pi^0\pi^0$; and, c) and d) $D_s \to \eta\pi^+\pi^+\pi^-$, where $\eta \to \gamma\gamma$.

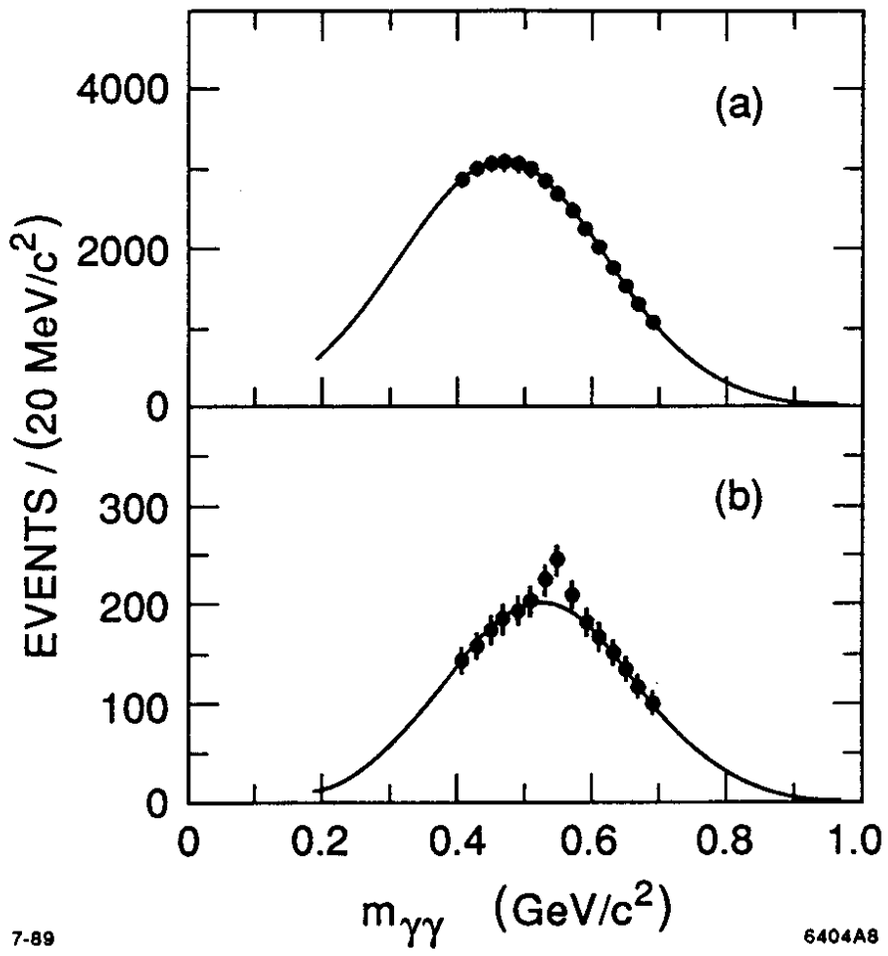

Figure 30: The effect of improved γ energy resolution and detection efficiency on the search for the rare (br 1.5 10^{-5}) decay $\tau^- \rightarrow \pi^-\eta\nu_\tau$[12]. The curves show the $\gamma\gamma$ mass spectrum of the candidate events in a detector with: a) a sampling electromagnetic calorimeter with $8\%/\sqrt{E}$ energy resolution and a detection efficiency of 50% at 50 MeV; and, b) a crystal electromagnetic calorimeter with $2\%/\sqrt{E}$ energy resolution and a detection efficiency of 50% at 10 MeV.

Examples of the improvement in physics sensitivity provided by such a calorimeter are shown in Figures 29 and 30. Note in Figure 29 that improved energy resolution both sharpens the reconstructed D mass *and* reduces the level of background (since tighter cuts can be made on π^0 and η candidates). A high resolution and efficient electromagnetic calorimeter is necessary in order to single-tag $\tau^+\tau^-$ events with the $l + E_{miss}$ signature; without such a calorimeter, the detector would lack sufficient resolution and hermeticity to isolate the events containing ν's.

3. **Excellent $\pi^{\pm}$, $K^{\pm}$ and p separation**, with $\leq 10^{-2}$ misidentification probability below 1 GeV/c.

4. **Excellent e and μ identification**, with $\leq 10^{-3}$ probability of misidentifying hadrons as electrons, and a few x 10^{-2} probability for π/K to be identified as μ.

5. **Hermeticity of the detector**, allowing for ν detection by missing energy. This can be achieved with an outer hadron calorimeter (tagger) and by eliminating blind regions in both the electromagnetic and hadronic calorimeters. The primary function of the hadron calorimeter is to tag the presence of neutral hadrons (K^0_L/n) which, if left undetected, would generate a background to the ν signal. After excluding such events, a precise determination of the missing energy can be made from the electromagnetic calorimetry and momentum measurements combined with particle identification. The detection inefficiencies are required to be below 1% in the electromagnetic calorimeter and below 5% in the hadronic calorimeter.

6. **Maximum-possible solid angle subtended in the barrel region.** This results in a large acceptance for the region of uncompromised performance: full tracking, precise σ_p/p, no end plate material, no detector boundaries, etc. The design goal is: Ω (barrel) $\simeq$ 90% x 4π str.

7. **Conservative (wide) interaction-region vacuum chamber**, with a radius (50 mm) that is identical to the aperture elsewhere in the storage rings. This avoids the impedance and heating problems that can result from a narrow vacuum chamber at the interaction region of a high-current storage ring. A further advantage is that the angular resolution of charged tracks *improves* with a large-diameter vacuum chamber, after connecting the vertex with the impact point at the vacuum chamber wall.

8. **Advanced trigger/data acquisition system and off-line analysis farm.** Although the event rate off-resonance is low ($\leq$ 10 Hz), at J/ψ it is several kHz, which implies the need for sophisticated triggering and a high-speed data acquisition system[32]. This will will generate a large amount of data which will require a dedicated off-line analysis farm similar to the ACP at FNAL[33].

7.2 Basic configuration

Following the previous considerations, we arrive at the basic configuration for the τcF detector dimensions (Figures 31 and 32). The dimensions in this figure and in the following

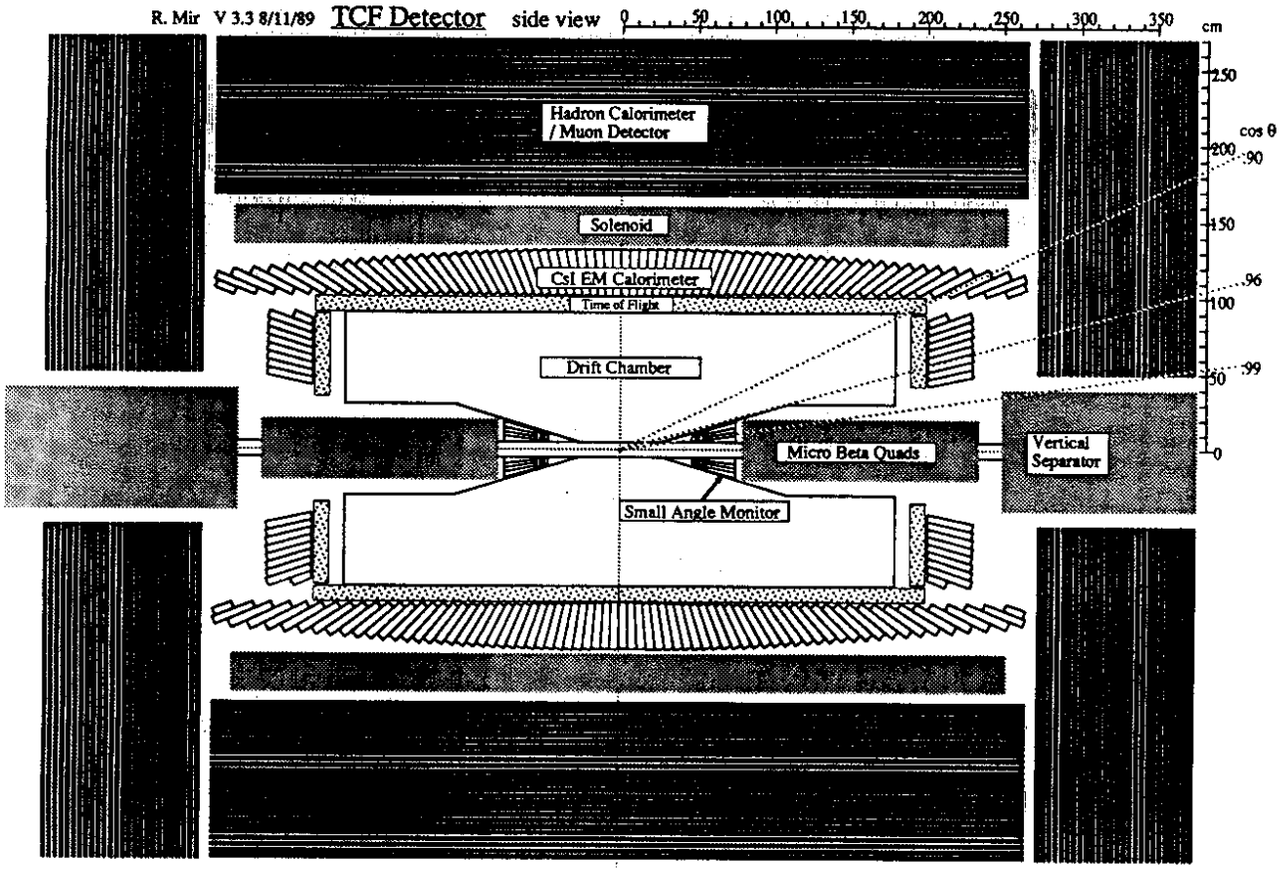

Figure 31: The basic configuration of the τcF detector (side view). The primary rôle of the hadron calorimeter is to tag the presence of K_L^0/n, and not the traditional one of hadron energy measurement.

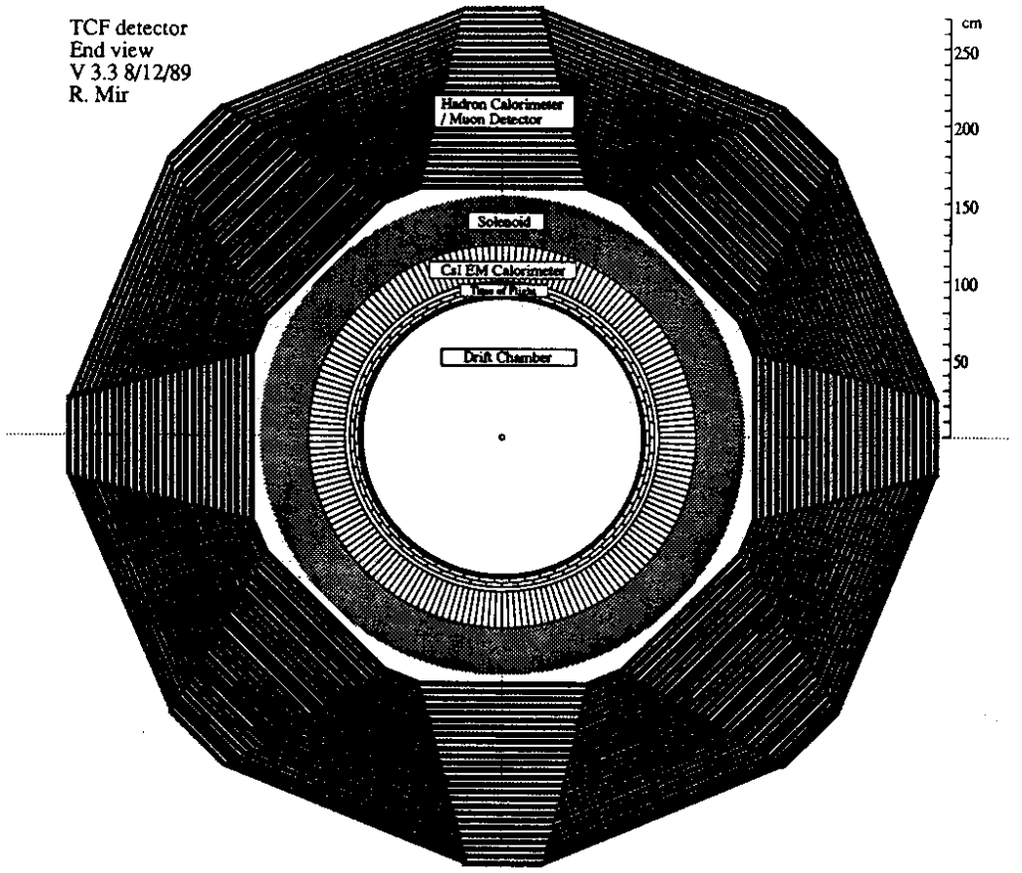

Figure 32: The basic configuration of the τcF detector (end view).

discussion should be considered as approximate, although they are probably within 15% of the optimized values. A brief initial specification of each component is as follows:

- **Magnet.** Given the requirement of a field strength in the range $1 \rightarrow 1.5$ T[31] and the extended operation foreseen for the τcF (10 months per year for a period of 10 or more years), the optimum choice for the solenoid is a superconducting, rather than warm, coil. The dimensions of the cryostat are: inner diameter 2.7 m, outer diameter 3.2 m, and length 5 m. With 1.5 T field, the stored energy is 160 MJ. The perpendicular thickness of the coil and cryostat is 0.9 rad.len. (0.20 λ_{abs}).

- **Tracking detector.** Since the free space between the $\mu\beta$ quads is only 1.60 m, they project inside the volume of the tracking detector. In order to accommodate this constraint, the wires taper to shorter lengths as they approach the interaction point. This has the advantages of creating useful space for small-angle detectors and their readout, reducing the dc current on the innermost wires, and providing a trigger with natural selection of events from the z region near the interaction point.

  Depending on the strength of the magnetic field, the tracking detector extends to an outer radius of 70-90 cm, with a hit density of 1 per cm. The wire lengths are 3.6 m

or less. Measurement of the z coordinate is done by narrow-angle stereo since this is compatible with the low-gain requirements of dE/dx measurements.

The multiple Coulomb scattering term, $\sigma_p/p = 0.3\%/\beta$, places severe constraints on the amount of material that can be tolerated in the DC. In order to achieve the lowest possible material, it is planned[35] to use a He-based DC gas, such as 94% He : 6% C_3H_8 ($1/X_0 = 5\ 10^{-4}$ rad. len. per m, to be compared with $60\ 10^{-4}$ rad. len. per m for 50:50 Ar:C_2H_6). Furthermore, with the use of Al field wires and with careful reduction of their number, it is anticipated that the contribution from the wires will be $20\ 10^{-4}$ rad. len. per m (to be compared with $74\ 10^{-4}$ rad. len. per m for the Mark II DC wires). The total DC material will therefore represent $25\ 10^{-4}$ rad. len. per m. With this amount of material, the design performance for σ_p/p can be reached within the following range of values for the lever-arm and magnetic field[36]:

$$L_{DC}(B) = 0.60\text{m}(1.5\text{T}) \rightarrow 0.80\text{m}(1.1\text{T})$$

The He-based drift gas will result in a reduced precision of both position and dE/dx. This is due to the small deposition of ionization (6 ion pairs per cm in He, compared with e.g. 29 per cm in Ar). However, neither of these disadvantages is too serious. An advantage of this gas, in addition to superior momentum measurement at low energies, is a relatively small cross-section for synchrotron X-rays ($\sigma \propto Z^4$), which are potentially a major background source in tracking detectors at high-current e^+e^- storage rings.

The inner region of the tracking detector ($5 \leq r \leq 20$ cm) is foreseen as a precise drift chamber, whose functions are to measure accurately the track positions and angles close to the vertex, and to improve the measurement of tracks that emerge at small polar angles. This device has a close wire spacing and perhaps a different gas than the He-C_3H_8 of the central tracker. In this case, a thin membrane would separate the two gas volumes. The inner tracking detector uses the (0.8 mm thick) Be vacuum chamber as a spool piece for supporting the wire tension; the central tracker wire tension is carried by a thin outer cylinder.

Following the design specifications, the tracking detector has an extended barrel region that subtends 90% x 4π str., leaving small end-caps that cover 6% x 4π str. The inner face of each $\mu\beta$ quad is also instrumented, as described below, to bring the total detector coverage to 99.7% x 4π str.

- **Electromagnetic calorimeter.** Among the candidate materials for the calorimeter, CsI(Tl) probably represents the best choice. The advantages are as follows: acceptable cost (\$1.6 cm^{-3} for bulk purchases), large light yield (52 photons per keV, which results in good γ measurement at low energy; the photodiode equivalent noise is 0.6 MeV), a reasonably short radiation length ($X_0 = 1.86$ cm), a small temperature dependency of the light yield ($< 0.2\%/^0$C at 20^0C), and easy handling. The only disadvantage is a slow light emission ($\tau \simeq 900$ ns, with long tails; 5% of the light appears after 3 ms). However, this will not be a problem since the cell occupancy is low, and

the effects of synchrotron noise etc. can be eliminated by continuous monitoring of the pedestals. Until recently a further disadvantage of CsI(Tl) was its apparently poor radiation hardness: doses of only 1 Gy were found to decrease substantially the transparency, resulting in several tens of percent reduction of the detected light. New measurements[37] indicate that the previous poor performance was due to impurities in the CsI(Tl) meltstock and, if pure materials are used, no reduction in detected light has been observed up to 50 Gy, which is the maximum dose, so far, in the new measurements. In the τcF detector we expect maximum doses in the electromagnetic calorimeter of 1-10 Gy per year in the most exposed regions close to the vacuum chamber. The radiation hardness of CsI(Tl) is therefore adequate.

The calorimeter is arranged in a tower geometry that projects, with a small offset, towards the interaction point. This will eliminate blind regions of the calorimeter and ensure the detector is hermetic. Each crystal is $16X_0$ in depth and has an entrance face $\simeq$ 5 x 5 cm^2. Each tower is read out with two Si photodiodes mounted to a waveshifter-plate that covers the rear face.

Two novel features of the calorimeter were discussed at the Workshop. The first is an additional pair of photodiodes that read out the front face of each tower, thereby providing depth information to aid $e\pi$ separation. The second involves a position-measuring layer situated after 3-4 X_0. One possibility is to install a superlayer of scintillating plastic fibres, arranged in a zuv geometry and read out via an image intensifier/ CCD system. An alternative possibility is a layer of Si pads or strips. In addition to improving the γ angular accuracy, this layer would give timing information that would provide a strong rejection of photon backgrounds, such as those caused by neutron albedo from hadron interactions elsewhere in the detector.

- **Hadron calorimeter/ μ detector.** Situated outside the solenoid is a fine-grained hadron calorimeter whose functions are to tag the presence of K_L^0/n, to identify μ, and to provide a flux return path. This has a depth of 80 cm Fe, made from 2.5 cm thick plates, separated by tracking chambers of 1.5 cm thickness. The best choice is probably drift chambers with long drift gaps (10-20 cm). Data from these chambers are continually recorded on a FADC and read out when a trigger occurs. Separation of π/K from μ is achieved by a combination of precise range measurements and absence of interactions.

  The effect of the solenoid material on the performance of the hadron calorimeter is under study. It is not expected to be a problem since it is equivalent to a single plate of the calorimeter, and it occurs early in the μ range (300 MeV/c).

- **Time-of-flight (ToF) counters.** ToF counters are an important component of the trigger and particle identification. From the experience of CLEO II[38] and others, we expect a resolution of 120 ps is feasible. The newly-developed mesh phototubes from Hamamatsu appear to be capable of reaching this performance while operating inside a strong magnetic field. Use of these tubes would eliminate the present need for large light-guide holes in the hadron calorimeter, which would simplify the construction and improve the hermeticity.

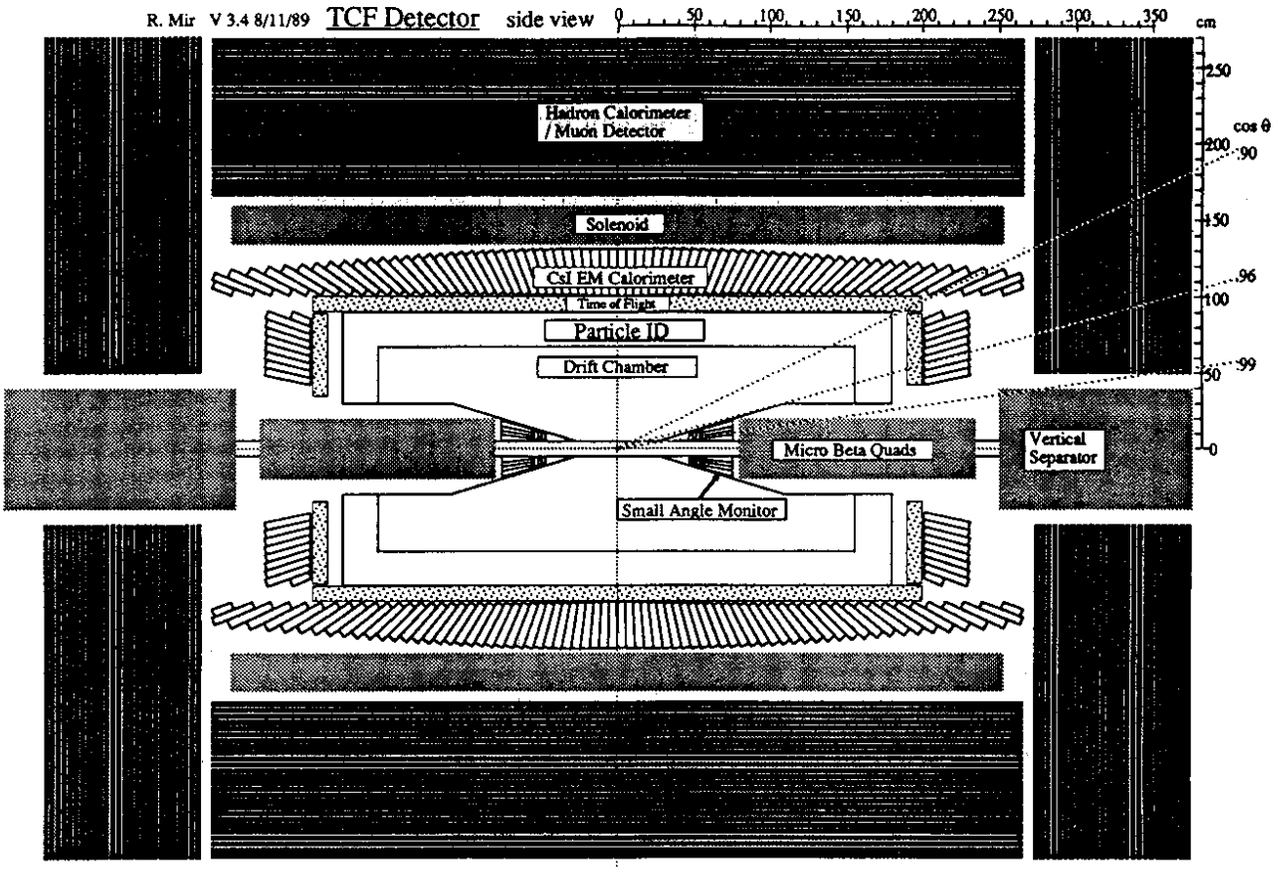

Figure 33: A modified version of the τcF detector with improved particle identification (side view). A space of approximately 20 cm is reserved between the drift chamber and the time-of-flight counters for a particle identifier. The dimensions of this version of the τcF detector with respect to the basic configuration are unchanged except for a reduction in the outer radius of the drift chamber. In order to maintain the design σ_p/p, there is a corresponding increase of the B field.

- **Small-angle detectors.** The inner face of each $\mu\beta$ quad is instrumented with an array of $16X_0$ BGO crystals, preceded by a tracking detector. These detectors complete the solid angular acceptance and provide the luminosity monitor. BGO is a good candidate due to its short radiation length (1.12 cm) and radiation hardness. The readout is identical with that of the central electromagnetic calorimeter. Another approach under consideration is a Si/W sampling calorimeter ($X_0 = 8$ mm).

7.3 Configuration with improved particle identification

Most τ-charm physics can be done with the particle identification capabilities of the basic τcF detector configuration; the kinematic limit of particles from $\tau^{\pm}$ and D decays is $\simeq 1$ GeV/c and so the identification of π, K and p is relatively easy using a combination of ToF and dE/dx.

The most stringent requirements on particle identification are made by the measurements of $D^o\bar{D}^o$ mixing and CP violation[20]. One important signature of mixing is $D^o\bar{D}^o \rightarrow (K^+\pi^-)_{D^0}(K^+\pi^-)_{\bar{D}^0}$ + cc. A fake signal can be generated if *both* the K and the π from a single D^0 are misidentified. The momenta of these particles are in the range $0.8 \rightarrow 1.0$ GeV/c where the separation relies purely on ToF. If we assume a 1% misidentification probability, then the fake rate will be $2\ 10^{-4}$, which constitutes the limiting experimental sensitivity to a mixing signal. These experiments will also use semileptonic decays to tag the charm flavour in a study of the charge composition of dilepton decays. Since there is a four-fold increase in data if both μ and e can be used (ee, $e\mu$ and $\mu\mu$), μ detection is worth a special effort.

In view of experiments such as these, which require extremely clean particle tagging, a second τcF detector configuration with enhanced particle identification is being studied (Figure 33). The idea is to introduce an additional detector layer that will both reduce the overall misidentification probability and provide some redundancy, so that the validity of a signal can be internally verified. A 20 cm space between the central tracking chamber and the ToF counters is sufficient for several options, such as a dedicated dE/dx device, improved ToF or a Cerenkov Ring Imaging Device (CRID).

The most serious tradeoff in this scheme is the introduction of material (up to 20% rad. len. in the case of a CRID) in front of the electromagnetic calorimeter. This would result in deterioration of the energy resolution of $\simeq$ 20% of the photons (those which converted before the calorimeter). There would also be a reduction in the detection efficiency of photons at the lowest energies, e.g. 20% reduction at 10 MeV. However, as indicated in Table 10, reduced photon peformance would be not be a problem for certain experiments, such as $D^o\bar{D}^o$ mixing and CP violation. In others, where photon detection is crucial, the particle identifier could be removed and the τcF detector operated with either an empty gap or an additional, low mass, tracking detector.

The differences in cost and performance of the two designs, with an empty gap in the second, are probably not significant. However, the second design has the important advantage of the potential to upgrade the particle identification. Flexibility for upgrading is an important consideration in large expensive detectors such as this, which are foreseen to have a long ($\geq$ 10 year) lifetime. This flexibility must be factored into the detector design at the outset.

The particle identifier may be based on present techniques or even future ones that could develop during the lifetime of the detector. Some of the present options are discussed below.

7.3.1 dE/dx in gaseous detectors

The dE/dx particle separation in CLEO II is shown in Figure 34. This Figure illustrates how useful are dE/dx measurements to particle separation in the low-β region. Calculations[39] of the performance of He-C_3H_8 gas in the τcF detector (Figure 35a) indicate a performance close to that of CLEO II. We also find (Figure 35b) that a dedicated dE/dx particle identifier of 20 cm depth has almost equal performance. The combination of the dE/dx information from both devices will provide 3σ πK separation up to 800

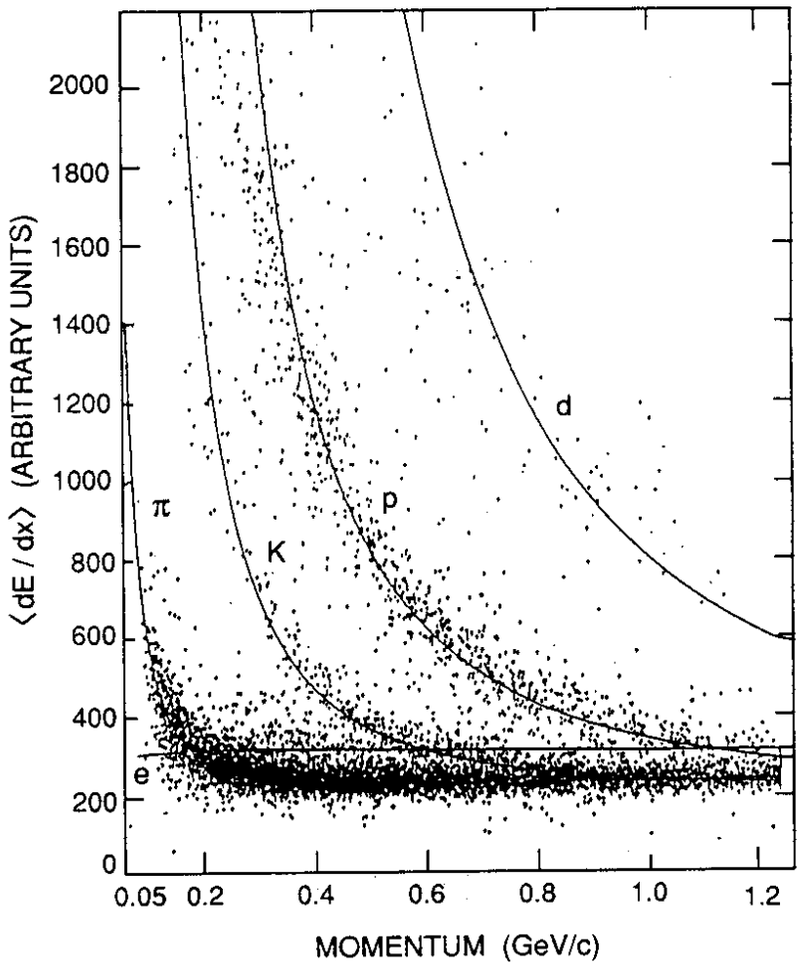

Figure 34: Mean energy loss in the CLEO II drift chamber [1 atm. Ar-C_2H_6, 72 cm, 51 samples, $(dE/dx)_{FWHM} = 14\%$]. The dE/dx resolution in the τcF detector is expected to be similar to these data.

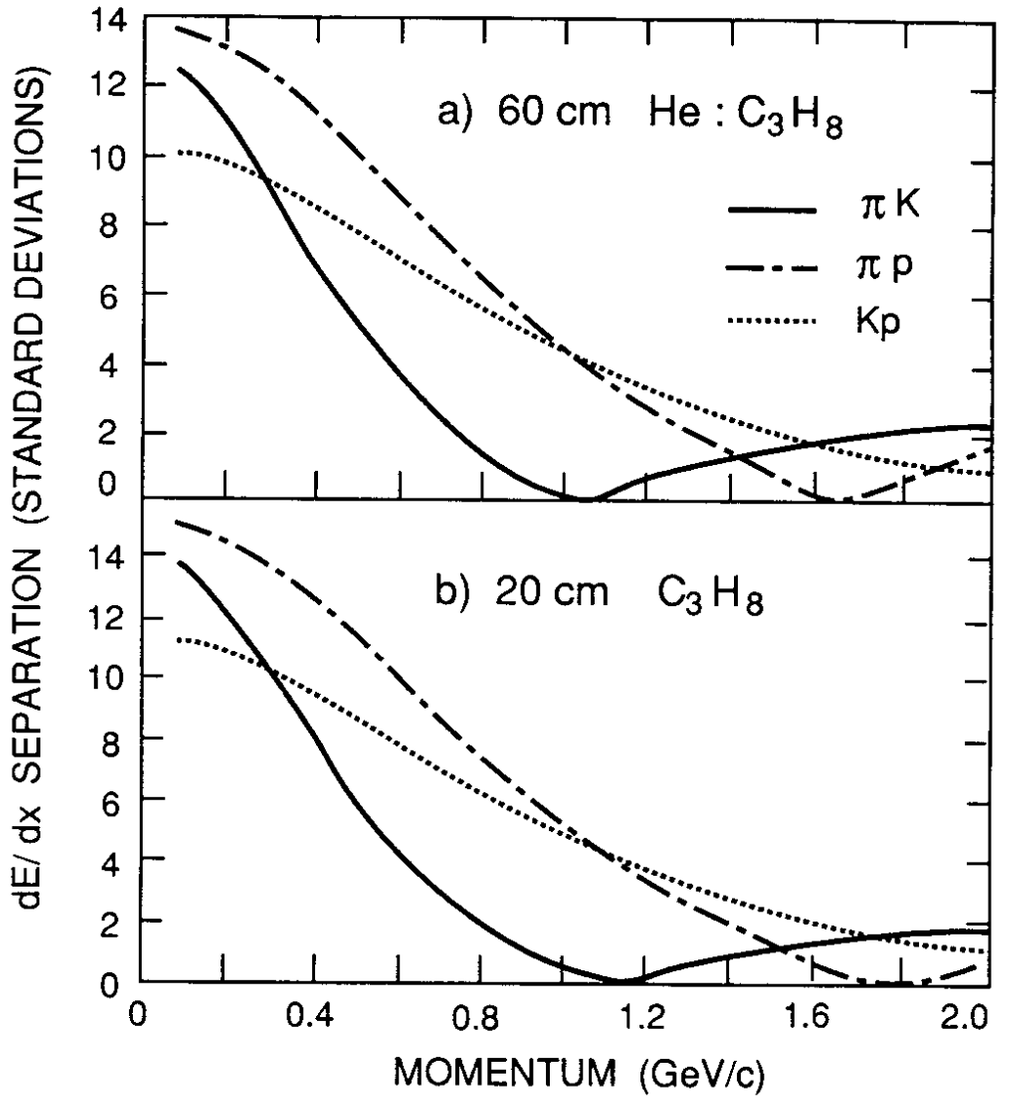

Figure 35: dE/dx hadron-hadron separation in the τcF detector: a) central tracking chamber (1 atm 93.8%:6.2% He-C_3H_8, 1 cm per sample, 60 samples); and, b) dedicated particle identifier (1 atm C_3H_8, 1 cm per sample, 20 samples).

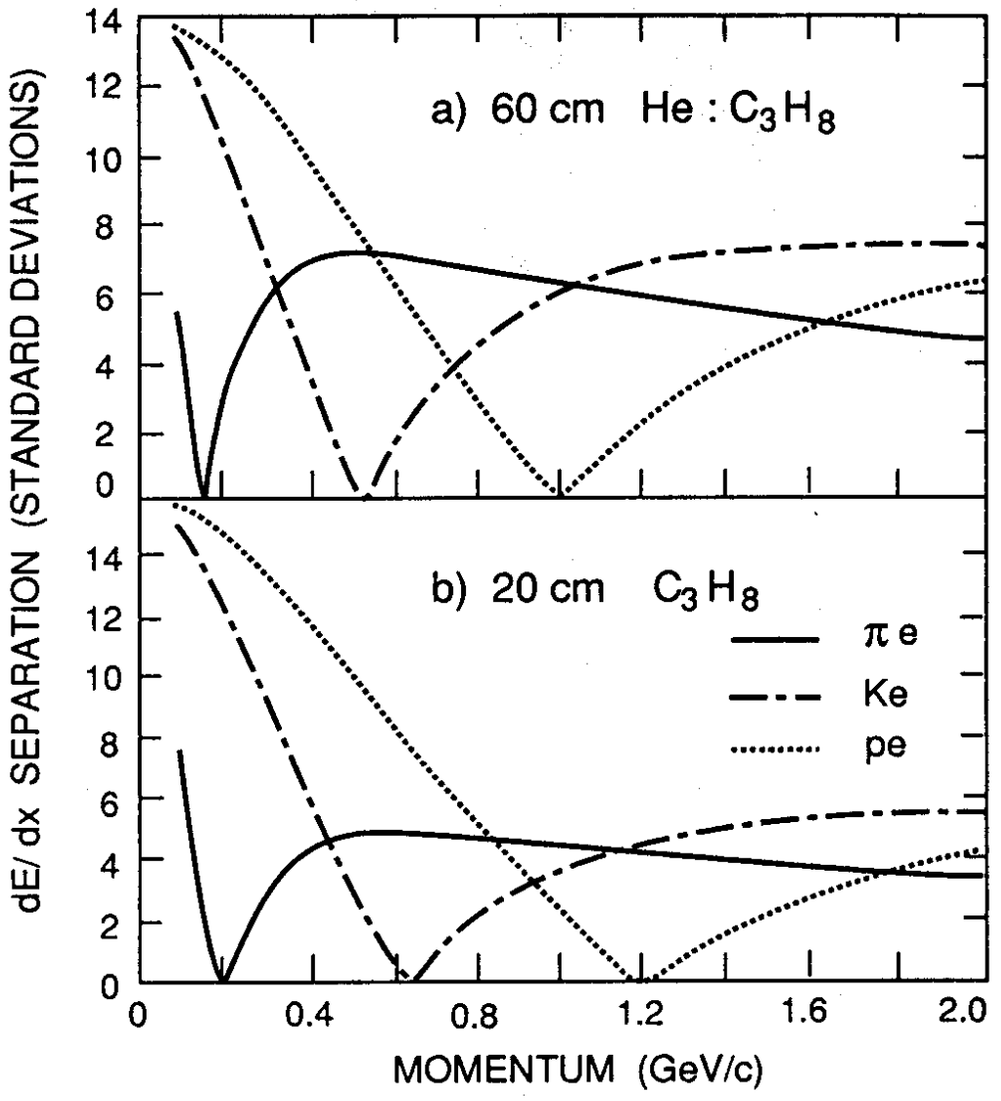

Figure 36: dE/dx hadron-electron separation in the τcF detector: a) central tracking chamber (1 atm 93.8%:6.2% He-C_3H_8, 1 cm per sample, 60 samples); and, b) dedicated particle identifier (1 atm C_3H_8, 1 cm per sample, 20 samples).

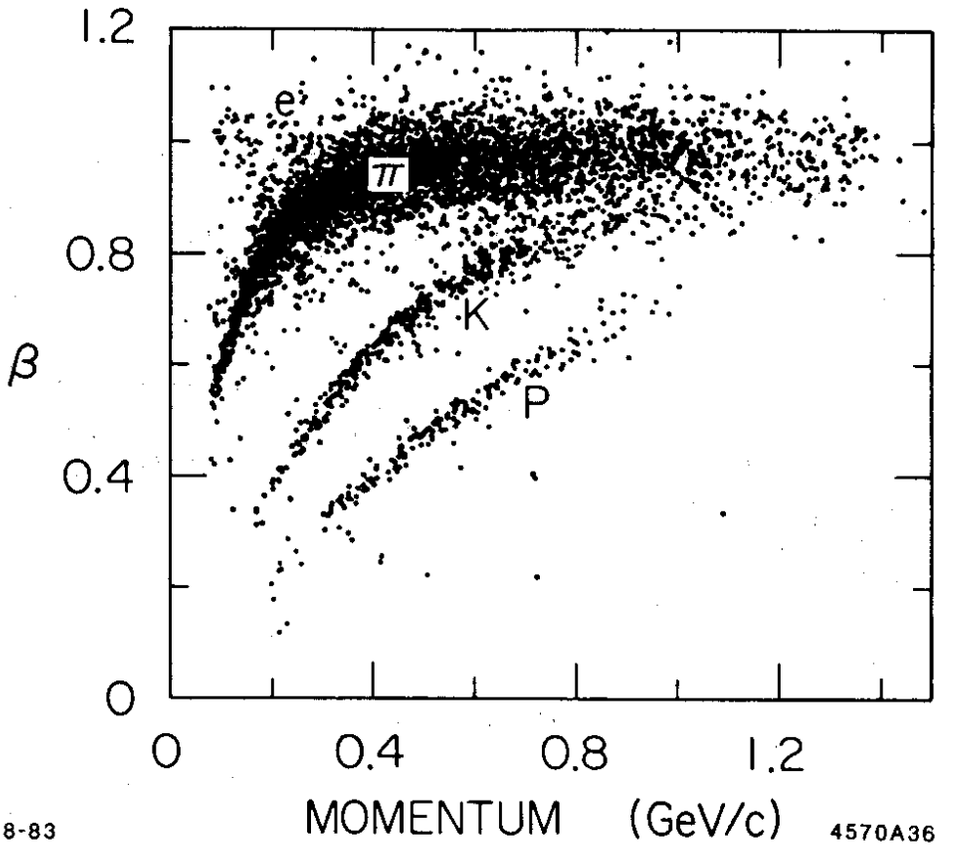

Figure 37: Time-of-flight particle separation in the Mark III detector at SPEAR (σ_{ToF} = 175 ps and minimum flight path = 1.2 m).

MeV/c. Useful hadron-electron separation is also provided, as shown in Figure 36.

7.3.2 Time-of-flight

The πK separation by ToF in the Mark III detector is illustrated in Figure 37. Particle separation by ToF is a relatively simple technique that has been highly successful at low energies, and there is a clear case to provide the τcF detector with the best possible timing resolution. The πK separation by ToF is shown in Figure 38[40]. In the τcF detector, the barrel ToF counters are located at a radius $\simeq$ 95 cm. Useful separation at 1 GeV/c therefore requires a timing resolution of 120 ps which, as discussed above, may be achievable with plastic scintillation counters of thickness 5 cm (12% rad. len.). The effects of energy loss in this material on the resolution of the electromagnetic calorimeter can be largely compensated by adding the energies measured in the individual ToF counters to the corresponding energies seen in the calorimeter.

7.3.3 Cerenkov ring imaging

A CRID with a liquid freon (C_6F_{14}) radiator is well-suited to particle identification in this energy range, as demonstrated in Figure 39[41]. This device would eliminate the difficulties

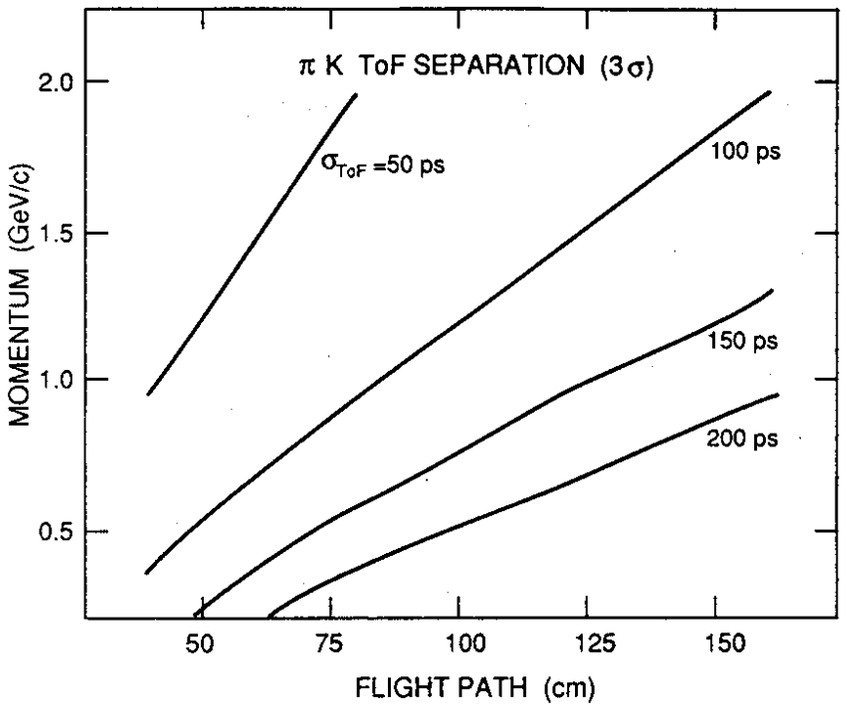

Figure 38: πK separation (3σ limits) by time of flight. Each curve corresponds to a different σ_{ToF}, as indicated.

	τcF	Mark III
Charged particles:		
Momentum resolution $[\sigma_p/p(\mathrm{GeV/c})]^2$	$[0.4\%p]^2 + [0.3\%/\beta]^2$	$[1.5\%p]^2 + [1.5\%/\beta]^2$
Angular resolution: σ_ϕ (mr)	1	2
σ_θ (mr)	3	11
Vertex precision: $[\sigma_{xy}(\mu\mathrm{m})]^2$	$[40/p(\mathrm{GeV/c})]^2 + [50]^2$	-
σ_z (mm)	1.5	15
p^π_{min}(MeV/c) for efficient tracking	50	80
Ω(barrel) (x4π str.)	90%	70%
Photons:		
Energy resolution $[\sigma_E/E(\mathrm{GeV})]^2$	$[2\%/\sqrt{E}]^2 + [1\%]^2$	$[18\%/\sqrt{E}]^2$
Angular resolution $[\sigma_{\theta,\phi}$ (mr)$]^2$	$[3/\sqrt{E}]^2 + [1]^2$	$[10]^2$
2γ angular separation $\Delta\theta_{2\gamma}$ (mr)	100	20
E^γ_{min}(MeV) for efficient detection	10	100
Particle identification:		
$h \to e$ rejection	$10^{-3} \to 10^{-5}$(+CRID)	4% at 0.5 GeV/c
$h \to \mu$ rejection	$4\%/p(\mathrm{GeV/c})$	5% at 1.0 GeV/c
$\pi \to K$ rejection	$10^{-2} \to 10^{-4}$(+CRID)	2σ at 1.2 GeV/c
K^0_L/n detection efficiency	95%	62%
E_{min}(MeV) for efficient ν tagging	$\simeq 100$	-

Table 11: Comparison of the performance of the τcF and Mark III detectors.

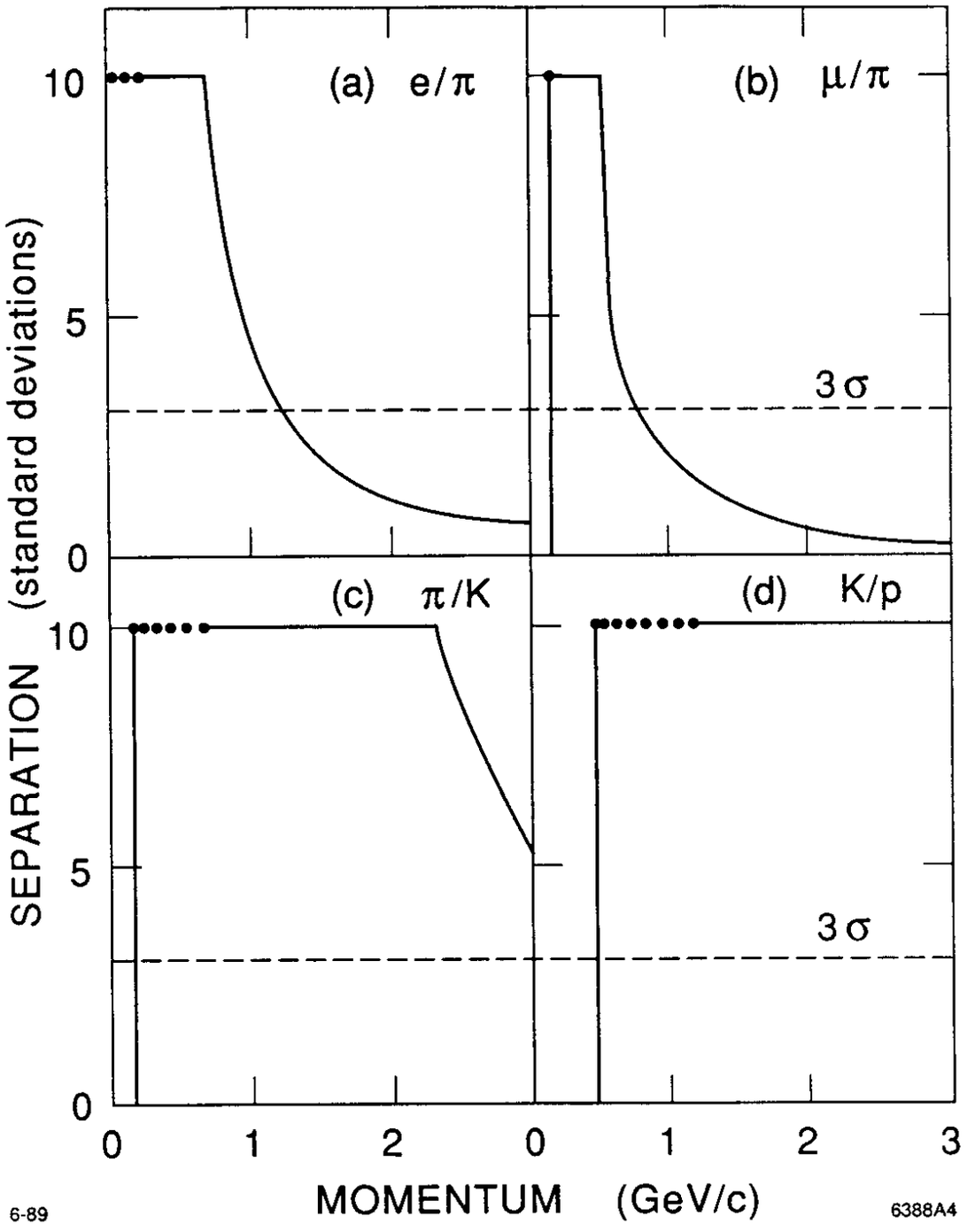

Figure 39: Particle separation in the CRID with a liquid freon (C_6F_{14}) radiator. The curves are considered to be saturated at 10σ. The dots correspond to regions where only the lighter particle emits Cerenkov light (i.e. threshold-counter discrimination). The low momentum cutoffs correspond to insufficient light emission from the lighter particle, in either the liquid radiator or quartz windows, to provide reliable separation. The separation is shown for: a) $e\pi$; b) $\mu\pi$; c) πK; and d) Kp.

in πK separation near 1 GeV/c. Moreover a CRID has excellent $e\pi$ and $\mu\pi$ separation at these energies. In particular it can provide strong $\mu\pi$ separation in the difficult low momentum region. As discussed above, the disadvantage is the large material: $\simeq$ 20% rad.len. With the startup of the large Cerenkov ring imaging detectors of DELPHI and the SLD, we will soon be able to see how well these detectors meet their promised high performances for particle identification.

7.4 Performance summary

Finally, we summarize in Table 11 the performance of the τcF detector in comparison with Mark III (or, equivalently, with the BES detector at BEPC, which has a similar performance to Mark III).

The elements of the τcF detector are similar to CLEO II, which has just started operation at CESR. In consequence, most of the detector components are well understood and will require little R&D prior to final design. The main differences of the τcF detector with respect to CLEO II reflect an optimization for τ-charm physics, notably: improvement of the momentum resolution at low energy, increase of the barrel solid angle, enhanced particle identification at low energies, and hermeticity with a fine-grained outer hadron calorimeter/ μ identifier.

8 Present status of the τ-charm Factory

Studies are taking place at several centres to consider the possibility of constructing a τ-charm Factory. These status of these studies ranges from individual initiatives to the preparation of detailed designs and formal proposals. In alphabetical order by nation, these centres are:

- *Orsay, France.* Machine and experimental physics groups are studying the τcF as a possible future option for the laboratory[42].
- *KEK, Japan.* A τcF machine design has been prepared[43] based on a double ring collider in the TRISTAN Accumulation Ring tunnel. A decision will be made on this kind of machine – either a τ-charm or a B Factory – in the near future.
- *Sevilla, Spain.* Initial discussions and planning towards the construction of the τ-charm Factory in Andalucia, near Sevilla, are well advanced[44]. This project would involve integral collaboration with CERN.
- *SLAC, USA.* Following the *Tau Charm Workshop*, a group of physicists[45] is proposing the construction of the τ-charm Factory at SLAC. A decision by SLAC between this project and a B Factory is expected before the end of 1989.
- *ITEP, Moscow, USSR.* The τ-charm Factory is being considered for construction at ITEP, Moscow, in collaboration with Novosibirsk[46].

9 Conclusions

In summary, the τ-charm Factory will explore, with unprecedented sensitivity, the third-generation τ and ν_τ leptons, the charm quark, and the decays of J/ψ and ψ'. In the context of the Standard Model, τ decays are completely predictable, and charm decays apparently give rise to uninspiring electroweak forces: V_{cs} and V_{cd} are largely determined by the Cabibbo angle, $D^0 - \bar{D}^0$ mixing is tiny, there is no observable CP violation and flavour changing neutral current decays are vanishingly small. We argue this makes the τ-charm Factory an ideal laboratory to confront the Standard Model with precise experimental tests; any deviation from the tightly constrained theory will be inescapable evidence for new physics.

There is no better way to pursue this physics than the τ-charm Factory, which promises an order-of-magnitude higher data rate than any other foreseeable machine, under optimal background and kinematic conditions. In addition to the large increase in machine luminosity, the performance of the τcF detector represents a substantial improvement in almost all respects relative to previous detectors in this energy range, especially with regard to electromagnetic and hadronic calorimetry.

Where are the major discoveries of tomorrow to be made? We do not know; perhaps there is a t quark at 150 GeV/c^2 or perhaps the ν_τ mass is 5 MeV/c^2? There is a democracy among machines whereby the new physics is not only found at the highest energy – it can spring up unexpectedly anywhere. Complementing the traditional exploration of the high-energy frontier, we foresee in the 1990's the increasing importance of a new breed of accelerator – the factory – which will explore the precision and rarity frontier of the known elementary particles. The τ-charm Factory is an inevitable component of this quest.

10 Acknowledgements

I would like to thank Manuel Aguilar-Benitez and my Spanish colleagues for organizing this stimulating meeting in a delightful setting – the fishing village of Lekeitio on the Cantabrian coast – and for the warm hospitality of our hosts at the Hotel Beitia. I also wish to thank my many colleagues who are developing the τ-charm Factory and, in particular, to acknowledge the pivotal contributions of John Jowett, Martin Perl and Juan Antonio Rubio. Finally, I would like to express my appreciation to Claude Rigoni for her cheerful and expert assistance in preparing figures for this paper.

References

[1] *Proceedings of the Tau Charm Workshop*, SLAC, California, 23-27 May 1989, eds. W.T.Kirk and M.L.Perl, SLAC-REPORT-343 (1989).

[2] M.Voloshin, *Topics in τ Physics*, talk presented at the SLAC *Tau Charm Workshop* (1989).

[3] A.Seiden, *Physics Summary*, ref. [1].

[4] J.M.Jowett, CERN LEP-TH/87-56 (1987).

[5] J.M.Jowett, CERN LEP-TH/88-22 (1988), Proc. *1st European Particle Accelerator Conference*, Rome, Italy, 1988 (World Scientific, Singapore, 1989) 368.

[6] J.Kirkby, *Backgrounds to τ studies below charm threshold*, ref. [1].

[7] J.J.Gomez et al., ref. [1].

[8] H.Harari and Y.Nir, Nucl. Phys. B292 (1987) 251.

[9] H.Albrecht at al., ARGUS, Proc. *XXIV International Conference on High Energy Physics*, Munich, F.R.Germany, 1988.

[10] Y.S.Tsai, SLAC-PUB-5003 (1989), ref. [1].

[11] F.Gilman and S.H.Rie, Phys. Rev. 31 (1985) 1066.

[12] K.K.Gan, ref. [1].

[13] A.Pich, these Proceedings, and ref. [1].

[14] R.Marshall, Proc. *XXIV International Conference on High Energy Physics*, Munich, F.R.Germany, 1988.

[15] B.Barish, ref.[1].

[16] C.A.Heusch, ref.[1] and Proc. *Les Rencontres de Physique de la Vallée d'Aoste*, La Thuile, Italy, 1989, ed. M.Greco.

[17] J.M.Izen, SLAC-PUB-4753 (1988).

[18] R.H.Schindler, ref.[1] and SLAC-PUB-4995 (1989), Proc. *Les Rencontres de Physique de la Vallée d'Aoste*, La Thuile, Italy, 1989, ed. M.Greco.

[19] I.I.Y.Bigi, ref. [1].

[20] G.Gladding, ref. [1].

[21] R.Willey, ref. [1].

[22] W.Toki, ref. [1].

[23] J.M.Jowett, *The τ-charm Factory Storage Ring; Initial Design and Parameters*, ref. [1].

[24] K.L.Brown, T.Fieguth and J.M.Jowett, *Machine Physics Summary*, ref. [1].

[25] G.A.Voss, J.M.Paterson and S.A.Kheifets, SLAC-PUB-5011 (1989), *Crab-crossing in a Tau-Charm Facility*, ref. [1].

[26] J.Kirkby, CERN-EP/87-210 (1987), Proc. *International School of Physics with Low-Energy Antiprotons, 2nd Course: Spectroscopy of Light and Heavy Quarks*, Erice, Sicily, 1987, eds. U. Gastaldi and R. Klapisch.

[27] K.L.Brown, SLAC-PUB-4366 (1987), Proc. *$B\bar{B}$ Factory Workshop*, UCLA, Los Angeles, California, 1987.

[28] T.Taylor, private communication.

[29] N.Kroll, ref. [1].

[30] S.Siemann, ref. [1].

[31] J.Kirkby et al., *Detector Summary*, ref. [1]

[32] J.Thaler, *Triggers at a τ-charm Factory*, ref. [1].

[33] K.Sliwa, *τ-charm Factory Data Acquisition and Offline Requirements*, ref. [1].

[34] P.Kim, private communication, and R. Schindler, ref. [1].

[35] A.Seiden and J.Va'vra, private communication.

[36] A.J.Weinstein, *Central Tracking Design for a τ-charm Factory*, ref. [1].

[37] D.Renker, Proc. *ECFA Study Week on Instrumentation for High Luminosity Hadron Colliders*, Barcelona, Spain (1989).

[38] M.S.Alam, private communication.

[39] J.Va'vra, *Particle Identification using dE/dx Technique*, ref. [1].

[40] R.Stroynowski, *Time of Flight Technique*, ref. [1].

[41] B.N.Ratcliff, *Design Considerations for a Cerenkov Ring Imaging Detector at the τ-charm Factory*, ref. [1].

[42] M.Davier, private communication.

[43] S.Kamada, talk presented at the SLAC *Tau Charm Workshop* (1989).

[44] J.A.Rubio, talk presented at the SLAC *Tau Charm Workshop* (1989).

[45] D.Coward, ref. [1], and B.Barish et al, SLAC-PUB-5053 (1989), contributed to the *XIV International Symposium on Lepton and Photon Interactions*, Stanford, California, 1989.

[46] M.Voloshin, private communication.